Polymer 54 (2013) 1269–1284

Contents lists available at SciVerse ScienceDirect

Polymer

journal homepage: www.elsevier.com/locate/polymer

Feature article

Inorganic block copolymer lithography

Adam Nunns, Jessica Gwyther, Ian Manners*

School of Chemistry, University of Bristol, Bristol BS8 1TS, UK

ARTICLE INFO

Article history:
Received 30 August 2012
Received in revised form
19 November 2012
Accepted 21 November 2012
Available online 28 November 2012

Keywords:
Block copolymer
Lithography
Self-assembly

ABSTRACT

Block copolymer lithography, a process where block copolymer self-assembly is integrated with conventional lithographic patterning, is emerging as a promising technology for addressing the future needs of the semiconductor industry. The ability of block copolymers to self-assemble into ordered nanodomains allows for simple, low cost nanopatterning into underlying substrates. Since its initial conception, block copolymer lithography has been demonstrated using a variety of block copolymers, with research primarily focusing on all-organic diblock copolymers. The most notable example is polystyrene-*block*-poly(methyl methacrylate) (PS-*b*-PMMA) where long-range ordering of nanodomains has allowed applications on a commercial scale. However, scaling down of the feature sizes produced from the self-assembly of organic block copolymers is often limited due to the relatively low Flory-Huggins interaction parameter, χ. In addition, etch selectivity between the blocks, and their etch resistance for subsequent pattern transfers steps, is generally low. This review article provides an overview of how the introduction of segments containing inorganic elements into block copolymers can help to address these issues and can also allow the direct deposition of functional materials such as metal nanoparticles. This has led to potential interest for the next generation of block copolymer lithography applications.

1. Introduction

A constant commercial drive for smaller, faster and more energy efficient electronic devices has demanded increased component density in integrated circuits, and hence smaller component sizes. The use of lithography in the semiconductor industry has been paramount to the successful development of integrated circuit technology, and the continual realization of Moore's law [1]. State-of-the-art techniques, such as immersion lithography [2] and double patterning [3], when combined with a 193 nm UV light source, have been used by leading chip manufacturers for the latest 22 nm-node technology. It is expected that these techniques will be used for the fabrication of future 14 nm-node technology. However, due to the inherent limit of the wavelength of UV light sources, combined with prohibitively high costs of implementing new technologies, photolithography might be abandoned in the future, for a surrogate lithographic process capable of producing sub-10 nm features [4–7].

Alternative processes to photolithography include electron-beam lithography [8], ion-beam lithography [9], X-ray lithography [10] and nanoimprint lithography [11]; all are top-down processes that rely on pattern transfer through masks or via molded stamps. Bottom-up processes have also garnered the attention of the semiconductor industry, as viable alternatives for the fabrication of nanoscale features.

Block copolymers (BCPs) are macromolecular materials comprised of two or more chemically different polymeric segments. As a result of their segmented structures BCPs have a propensity to phase-separate and order themselves into a range of complex morphologies on the nanoscale. In the simplest case of an AB diblock copolymer, the driving force for phase-separation is due to the free energy cost of contact between blocks A and B, as described by the Flory-Huggins interaction parameter, χ_{AB}. Several experimental methods have been used to determine χ between distinct polymers, including small angle neutron scattering (SANS) [12–16], ellipsometry [17], light scattering [18–20], melting point depression and comparison of solubility parameters [21]. It has been shown both theoretically and experimentally that χ_{AB} has an inverse relationship with temperature, and thus lowering the temperature of a BCP melt favors the reduction of A–B contacts leading to phase-separation. The degree of polymerization, *N*, of each block, also plays a significant role in determining whether a block copolymer will phase-separate into an ordered system, or remain disordered. At large *N*, it is thermodynamically preferable to minimize A–B contacts and phase-separate the blocks into separate domains, even at the cost of the associated loss in translational and configurational entropy.

* Corresponding author. Tel.: +44 (0)117 928 7650; fax: +44 (0)117 925 1295.
E-mail address: Ian.Manners@bristol.ac.uk (I. Manners).

0032-3861/$ – see front matter © 2012 Elsevier Ltd. All rights reserved.
http://dx.doi.org/10.1016/j.polymer.2012.11.057

Thus, it is the magnitude of χN that determines whether the block copolymer exists in an ordered (phase-separated) or disordered state. Above the order-disorder transition (ODT), where χN exceeds a critical value, denoted χN_{ODT}, the BCP phase-separates. The relative volume fractions (φ) of A and B determine the self-assembled morphology of the diblock copolymer, whereas the size of the domains is governed by the degree of polymerization of each block [22,23].

It is the ability of block copolymers to self-assemble into a range of morphologies that makes them suitable candidates for bottom-up lithographic processes. The infrastructure currently used in integrated circuit design is applicable for block copolymer lithography, with block copolymer films sharing many similarities with photoresist materials used in photolithography. The processability of BCPs in a variety of solvents allows polymer films to be spin-coated onto virtually any substrate, analogous to photoresist materials. The self-assembly of BCPs into ordered structures on the nanometer-scale allows for transferral of these features into an underlying substrate, via a plasma etch step. In this respect, they act as sacrificial templates, like conventional photoresist materials, but providing the template design in a bottom-up manner, saving the requirement of expensive optical set ups and complicated template designs.

Pattern transfer in block copolymer lithography relies on good etch selectivity between the coblocks. A reactive ion etch (RIE) step is commonly used to achieve pattern transfer into a substrate whereby the individual polymer segments degrade at different rates in the presence of different feed gas plasmas [24]. For example, when a thin film of polystyrene-*block*-polybutadiene (PS-*b*-PB) block copolymer is exposed to an ozone plasma, the unsaturated bonds along the PB backbone are cleaved, whilst the PS is cross-linked. Development of an ozone-exposed film leaves the cross-linked PS domains, which can be employed as a sacrificial mask for subsequent pattern transfer with a RIE step [25]. Similarly, exposure of a polystyrene-*block*-poly(methyl methacrylate) (PS-*b*-PMMA) film to UV light degrades PMMA whilst simultaneously cross-linking PS, allowing for the subsequent pattern transfer of the remaining cross-linked PS [26,27].

In a block copolymer system where $\chi N >> 10$, known as the strong segregation limit, the width of the interfaces separating block A from B can be described by $\alpha\chi^{-1/2}$ where α is the characteristic segment length of a monomer unit. Thus, block copolymers with a higher χ will exhibit sharper interfaces between each block, allowing for the creation of features with a smaller edge roughness if used in a lithographic process. Additionally, the period of the phase-separated microdomains can be described as $D \sim \alpha N^{2/3}\chi^{1/6}$. This implies that reducing N, whilst maintaining an appropriate χN over the critical value for phase-separation, would lead to smaller features with a smaller period [23].

Since the early work by Register, Chaikin et al. [28] demonstrating the use of polystyrene-*block*-polyisoprene (PS-*b*-PI) films to create an array of 10^{11} holes/cm^2 in Si_3N_4 [29], substantial advances have been made in the field of block copolymer lithography. This has enabled the fabrication of air-gap interconnects [30], capacitors [31,32], field effect transistors [33], flash memory devices [34,35] and ultra-high density magnetic-dot arrays [36]. Improving the long-range ordering of the phase-separated block copolymer domains, as well as the manipulation of their morphology, has been an important development in the field [37]. Nealey et al. demonstrated the fabrication of highly-ordered, nanometer-scale jogs, junctions and isolated lines, all essential for integrated circuit technology, from ternary blends of PS, PMMA and PS-*b*-PMMA on chemically patterned substrates [38]. Highly-ordered, square-packed arrays of holes in a silicon oxide substrate have been prepared via block copolymer lithography using a blend of poly(ethylene oxide)-*block*-poly(styrene-*r*-4-hydroxystyrene) and poly(methyl methacrylate)-*block*-poly(styrene-*r*-4-vinyl pyridine) [39]. Russell and co-workers utilized a sawtooth patterned substrate to produce a single grain of hexagonally arranged cylinders from thin films of polystyrene-*block*-poly(ethylene oxide) (PS-*b*-PEO), with exceptionally high orientational and translational order, over an area of ~4 cm^2 [40]. We direct the reader to a list of reviews describing many of the latest accomplishments in the field [34,41–45].

Whilst organic systems, such as PS-*b*-PMMA, PS-*b*-PI and PS-*b*-PB have been shown to be potential candidates for lithographic patterning, their relatively low χ-values limit both the scaling of domains to relatively large features, and also the definition of the domains created. Whilst organic block copolymer systems with high χ-values do exist, such as amphiphilic polystyrene-*block*-poly(4-vinylpyridine) [46,47] and PS-*b*-PEO [48], the low etch selectivity between the organic blocks hinders their potential. The incorporation of inorganic segments into block copolymers is an attractive prospect, as it addresses both of these issues. Inorganic–organic BCPs tend to have higher χ-values and greater etch selectivity between the blocks, due to the formation of robust oxide surface layers within the inorganic polymer domains when exposed to an oxygen plasma. The introduction of inorganic blocks also offers the potential for materials with useful physical or chemical properties to be directly fabricated from the BCP film, giving functional, as opposed to sacrificial, resist materials, thereby reducing the number of required steps for device fabrication. This review will focus on the introduction of inorganic segments into block copolymers for lithographic applications.

2. Silicon-containing block copolymers

2.1. Poly(dimethylsiloxane)-containing block copolymers

The introduction of silicon into a segment of a BCP has several advantages in the field of block copolymer lithography. Firstly, exposure of a silicon-containing polymer to an oxygen plasma leads to the formation of SiO_x species at the polymer/plasma interface, which gives far greater etch resistance than a solely organic polymer. Poly(dimethylsiloxane) (PDMS), a polymer comprised of a Si–O backbone, has been combined with various organic blocks as a means of patterning substrate layers. As noted previously, BCPs with a larger χ can phase-separate at lower N, giving smaller domains with a smaller period. Sharper interfaces between the phase-separated blocks are also obtained, resulting in a lower edge roughness of the patterned features. For PS-*b*-PMMA, $\chi = 0.04$–0.06 [49], whilst for PS-*b*-PDMS, $\chi = 0.26$ [50]. Thus, for a PS-*b*-PDMS diblock copolymer, phase-separation can be achieved with a lower degree of polymerization, allowing for the potential fabrication of smaller, more well-defined features with a smaller period. This behavior can also be described in terms of the difference in solubility parameters between each homopolymer, which is correlated to the value of χ [51].

Work by Chen, Fu et al has focused on self-assembled thin films of PS-*b*-PDMS for potential use as nanolithographic templates. Solutions of PS-*b*-PDMS were spin-coated onto silicon wafers, and solvent annealed in either THF or acetone to give a monolayer of spheres of PDMS in a matrix of PS, where a PS layer is formed at both the air/polymer and polymer/substrate interfaces. Subsequent exposure to UV irradiation combined with ozonation (UV/O_3) removed the PS matrix and gave a hexagonally-packed monolayer of PDMS spheres [52]. It was also demonstrated that addition of PS homopolymer to the sphere-forming PS-*b*-PDMS before solvent annealing allowed for greater long-range ordering to be achieved in a shorter annealing time [52,53].

Exchanging PS for polylactide (PLA) results in a greater χ-value when paired with PDMS ($\chi_{PDMS\text{-}PL} \approx 0.94$ at 298 K, calculated from the difference in the Hildebrand solubility parameters of PLA and PDMS [54]). Hillmyer et al. prepared thin films of cylinder-forming PDMS in a PLA matrix, using a symmetrical PLA-*b*-PDMS-*b*-PLA block copolymer [55]. Solvent annealing of a thin film of PLA_{13}-*b*-$PDMS_8$-*b*-PLA_{13} (subscripts denote molar mass of each block, in kg mol^{-1}) in toluene gave cylinders of PDMS perpendicular to a Au-capped Ni/Cr substrate, measuring 28 nm in diameter, with a domain spacing of 36 nm, as determined by SAXS. A SF_6 RIE completely removed the PDMS domains, resulting in a nanoporous film of PLA, with comparable ordering to the pre-etched film. Conversely, exposure of the films to an O_2 RIE resulted in complete removal of the PLA matrix, giving SiO_x dots, again with comparable ordering to the pre-etched film. Pattern transfer of the nanodot silica array into the Au substrate was achieved by subjecting the film to 60 s of argon ion beam milling, revealing Au dots on a Ni/Cr substrate, with a diameter of 18 nm and domain spacing of 27 nm (Fig. 1).

A relatively new technique for achieving directed self-assembly of PDMS-containing block copolymers, nanoimprint lithography, has been demonstrated for the fabrication of sub-10 nm features [56,57]. Ordering is achieved through graphoepitaxy of the block copolymer, where artificial topographic features are used to induce alignment of the PDMS cylinders, in this case parallel to the imprint mold sidewalls. The predominant issue with nanoimprint lithography, whether for directed self-assembly of BCPs or for direct pattern imprint into films, is of mold release. Without efficient release of the imprint mold, the features created by the technique lose their integrity, giving unreliable and non-reproducible patterning, whilst simultaneously coating the mold and adding further cleaning steps to the procedure [57]. Further requirements for directed self-assembly of BCPs involve the preferential wetting of the desired polymer to the surface of the mold, to aid graphoepitaxy whilst giving efficient mold release afterwards.

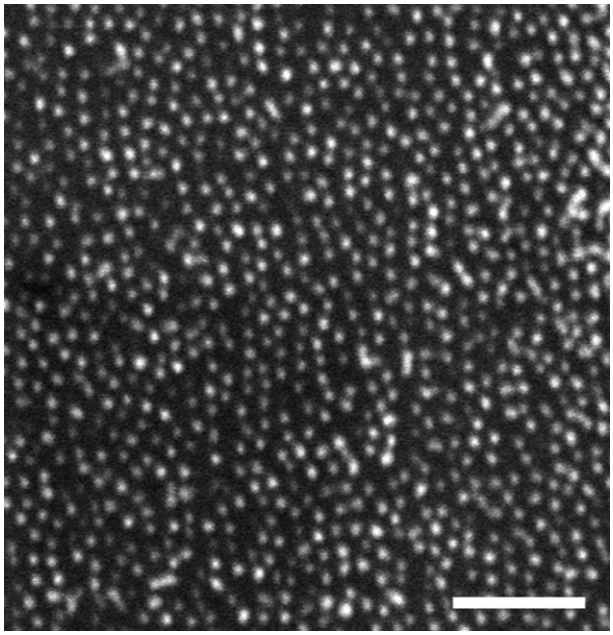

Fig. 1. SEM image of a Au dot array produced from thin films of PLA_{13}-*b*-$PDMS_8$-*b*-PLA_{13} (subscript indicates molar mass of each block, kg mol^{-1}) which has been solvent annealed for 45 min and subsequently exposed to 150 s O_2 RIE and 60 s Ar ion beam milling. Au dots (bright) are observed on a Ni/Cr substrate (dark). Scale bar 200 nm. Reproduced with permission from Ref. [55]. Copyright © 2010, American Chemical Society.

The approach taken by Olynick, Helms and co-workers to ensure efficient mold release was to coat the imprint mold with a layer of material that aids release from the patterned film [56]. Fluoroalkyl-modified PS and PDMS (FA-PS and FA-PDMS, respectively) were tested, with FA-PS giving significantly better results. A 5% w/w loading of FA-PS on the mold, with respect to the PS-*b*-PDMS film, was found to be optimum for efficient mold release and graphoepitaxy of the BCP film. Further work showed that PDMS-coated imprint molds gave enhanced performance over FA-PS, especially within a corrugated mold pattern [58]. This was surprising, as the interfacial energy between the PDMS-coated mold and substrate, calculated from the estimated work of adhesion for substrates and mold interfaces, was found to be greater than that of the FA-PS-coated mold. The enhanced performance was attributed to PDMS having a lower peel-fracture than perfluoro groups, potentially giving lower friction losses than that of FA-PS, when the mold is removed from the patterned film [59–61].

In order to achieve directed self-assembly of PS-*b*-PDMS films, solutions of the BCP were spin-coated onto a silicon substrate with a PS brush layer. This gave preferential wetting of the PS domain at the polymer/substrate interface. Thermal nanoimprinting with a PDMS-coated mold was performed at ~50 psi, at 200 °C for 1 h, by attaching the mold and substrate to two parallel metal plates. The system was allowed to cool to room temperature over 1 h, before the mold was removed in a direction normal to the substrate. A 5 s CF_4 RIE was used to remove the PDMS surface layer of the film, exposing the PDMS cylinders and PS matrix, the latter of which was removed by a further 10 s O_2 RIE, giving highly-ordered, 8 nm lines of SiO_x with a period of 20 nm (Fig. 2).

Avgeropoulos, Ho and co-workers [62] have shown that through careful manipulation of the surface of a PDMS-cylinder forming PS-*b*-PDMS block copolymer film, ordered arrays of nanorings, potentially useful in magnetic memory devices [63], can be produced. Solvent annealing of spin-coated thin films in toluene gave perpendicular PDMS cylinders in a matrix of PS, with respect to the substrate. Surface reconstruction of these films was achieved by immersion of the BCP film in dodecane for 12 h. The surface tension of PDMS is lower than PS, thus immersion of the BCP film in dodecane, a selective solvent for PDMS, induces increased chain mobility causing it to migrate from within the PS matrix to the air/polymer interface. The PS matrix remains intact, leaving a nanoporous thin film. After removal of the PDMS surface layer by treatment of the films with a CF_4 RIE step (10 s), a core-shell cylinder morphology was obtained. Treatment of this film with an oxygen plasma produced a thermally and mechanically robust silicon oxicarbide (SiOC) nanoring array, which could be used as a mask for further pattern transfer.

In an alternative approach, a free-standing nanoporous SiOC mask was prepared from a PS-cylinder forming PS-*b*-PDMS BCP [64]. Thin films were prepared by spin-coating a 1 wt% solution of the BCP from a dodecane solution onto a carbon-coated glass slide. The glass slide was treated with an HF solution, the polymer film suspended in water and then deposited onto a copper TEM grid. This provided a solid support through which both sides of the film could be treated with an oxygen plasma, removing the PS domains and carbon film, whilst simultaneously oxidizing the PDMS domains, to produce a nanoporous SiOC mask. Subsequently, 30 pattern transfer processes of the same hexagonally-packed cylindrical nanoporous mask into underlying polymer substrates (PS, PMMA, polycarbonate) were demonstrated, with no significant change in the integrity of the mask.

Further research into using PS-*b*-PDMS as a nanolithographic mask has been performed by Ross et al., whom have demonstrated unprecedented control over the morphology of the self-assembled

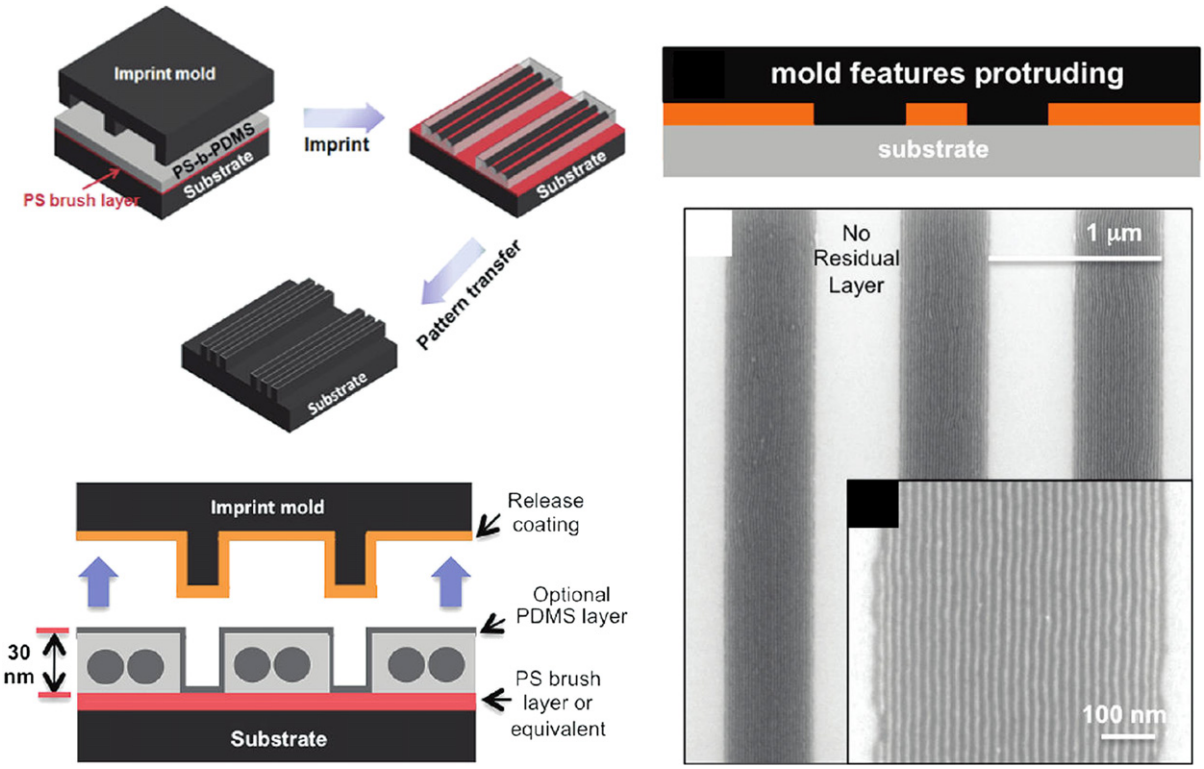

Fig. 2. Left – Schematic showing the nanoimprint lithography process. Right – SEM image showing O_2 plasma etched BCP film after the nanoimprint process. Inset shows magnified oxidized PDMS cylinders aligned parallel to the sidewall of the imprint mold. Reproduced with permission from Ref. [58]. Copyright © 2011, American Chemical Society.

films, and their long-range order. Initially, directed self-assembly of the materials was achieved through solvent annealing of the polymer thin films on pre-patterned, surface-functionalized substrates with linear trenches [65]. It was found that a PDMS brush layer on the silicon substrate gave the greatest degree of ordering of the polymer, giving parallel cylinders of PDMS in a matrix of PS. A thin, continuous layer of PDMS also forms at the air/polymer interface, owing to its lower surface tension compared to PS [66]. In order to reveal the underlying PDMS cylinders, the films were exposed to a 5 s CF_4 RIE. The orientation of PDMS cylinders, parallel or perpendicular to the linear trench walls, can be controlled by adjusting the relative widths of the mesa (the gap between each trench) and trench in the substrate, and through different solvent vapor pressures in the annealing process. A greater W_{mesa}/W_{trench} ratio and relatively low vapor pressure in the annealing process was found to favor the formation of perpendicular cylinders, relative to the trench sidewall.

An ethanol vapor sensor was prepared from a patterned film of poly(3,4-ethylenedioxythiophene):poly(styrenesulfonate) (PEDOT:PSS), a conducting polymer. 15 nm wide conducting nanowires with a 35 nm period, ordered over several cm^2, were fabricated by block copolymer lithography, using a highly-ordered, cylinder-forming PS-*b*-PDMS block copolymer as a sacrificial mask. The process is outlined in Fig. 3. Fabrication of such sensors demonstrates the great potential of block copolymer lithography in the fabrication of active devices [67].

Directed self-assembly of the same polymer in circular pits gave concentric ring patterns of PDMS cylinders; the number of rings being governed by the diameter of the pit. Double-rings of Co were fabricated by sputtering Co onto O_2 plasma-etched rings of PS-*b*-PDMS, followed by a CF_4 dry etch step to reveal the Co rings [68]. Such nanoring arrays could be used to lower power consumption of, increase information density storage of and/or give faster switching times in devices which already incorporate nanorings, such as transistors, memories, sensors, quantum devices and lasers [63,69–76].

As discussed above, phase-separation of PS-*b*-PDMS occurs at lower molecular weights than PS-*b*-PMMA block copolymers owing to the high χ-value for the PS-*b*-PDMS. This allows for fabrication of smaller features when PS-*b*-PDMS is used in block copolymer lithography. Highly-ordered 8 nm lines of SiO_x, with a period of 17 nm, have been fabricated from a PDMS-cylinder forming PS-*b*-PDMS block copolymer with a molecular weight of 16 kg mol^{-1} (Fig. 4a). Nanowires of tungsten with a width of 9 nm were then made by sputtering a 55 nm thick tungsten layer onto the SiO_x line array, followed by CF_4 sputtering to remove the excess tungsten. Once the buried SiO_x patterns are reached, they are removed more rapidly than then tungsten, giving the reverse-pattern of tungsten lines (Fig. 4b) [77]. The same process was used to produce Ti, Pt, Co, Ni, Ta, Au and Al nanowires [78].

Subsequent work by Ross and co-workers has focussed on the nature of the graphoepitaxial template for the directed self-assembly of PS-*b*-PDMS. Trenches were replaced with sparse arrays of hydrogen silsesquioxane (HSQ) posts functionalized with a PDMS brush layer. The brush layer allows the posts, which are a similar diameter to the PDMS domains, to act as surrogate PDMS spheres or cylinders in the block copolymer film, dramatically improving long-range ordering of the BCP. Templates were prepared by spin-coating solutions of HSQ onto a silicon wafer, which is then patterned by scanning electron-beam lithography [79]. Exposure of specific sites to the electron-beam causes cross-linking, producing a silica-like material [80]. The unexposed film is removed during development, leaving the desired nanopost array behind. The post array is designed to be commensurate with the equilibrium periodicity of the block copolymer domain spacing, to ensure that optimum graphoepitaxy is achieved.

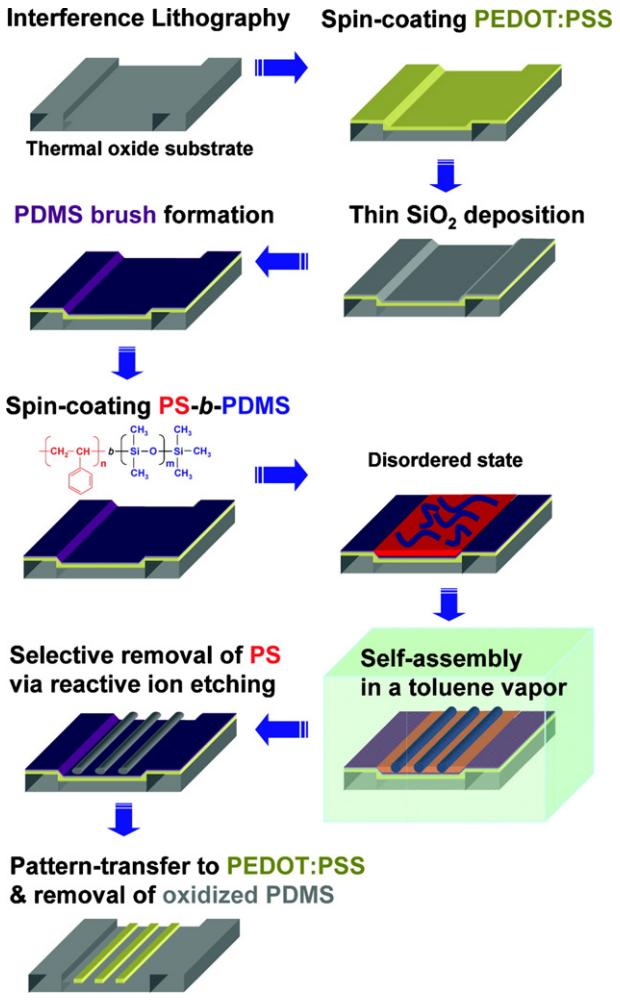

Fig. 3. Schematic of the procedure used for the fabrication of a conducting PEDOT:PSS nanowire array. Reproduced with permission from Ref. [67]. Copyright © 2008, American Chemical Society.

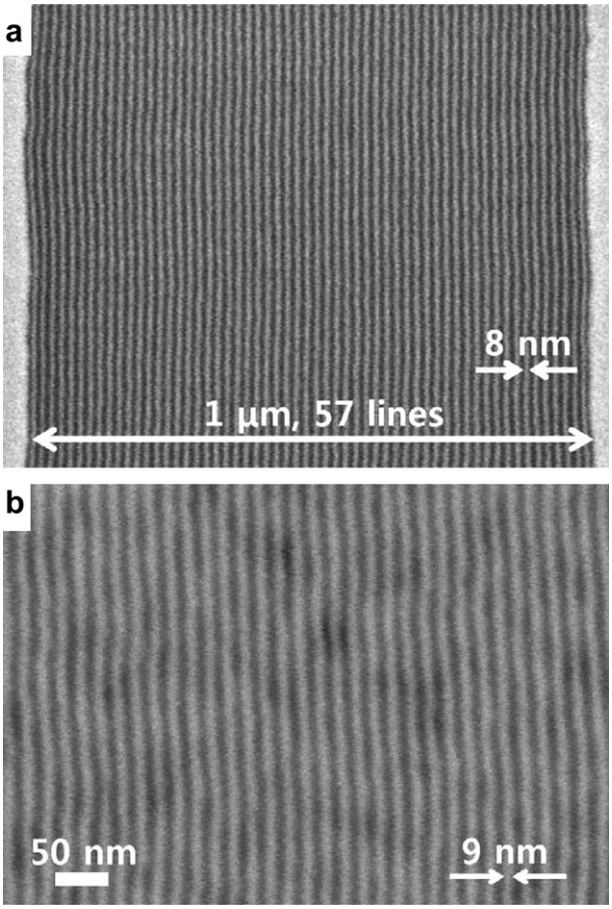

Fig. 4. a) SEM image of an O_2 plasma etched PS-*b*-PDMS film, showing highly-ordered cylinders of SiO_x aligned parallel to the trench wall. b) SEM image of a tungsten nanowire array fabricated via BCP lithography, using a 16 kg mol^{-1} PS-*b*-PDMS film. Reproduced with permission from Ref. [77]. Copyright © 2011, American Chemical Society.

Spin-coating a PDMS-sphere forming PS-*b*-PDMS block copolymer onto a sparse, hexagonal array of HSQ posts, followed by thermal annealing at 200 °C, a short CF_4 then O_2 RIE, revealed a highly-ordered hexagonally-packed array of SiO_x spheres [79]. The spheres pack around the HSQ posts, which act as surrogate domains, filling the position where a PDMS sphere ought to be, thus guiding the self-assembly of the polymer over a long range, as shown in Fig. 5. For a [30] triangular array of HSQ posts (where the notation used to describe the location of the surrogate HSQ posts is analogous to the two-dimensional Miller indexing system used in crystallography), that is, where $L_{post}/L_o = 3$, defect free arrays of PDMS spheres were observed over areas $>2\ \mu m^2$. When compared to a non-templated film, where the largest defect area observed was $\sim 0.4\ \mu m^2$, the power of this method becomes apparent.

Whilst fabrication of periodic arrays of nanoscale features, through block copolymer lithography has been demonstrated via many routes, the fabrication of aperiodic features, such as junctions, jogs and bends, essential in integrated circuits, remains a challenge. By changing L_x and L_y, relative to L_o, on a HSQ post array template, self-assembly of the PS-*b*-PDMS can be adjusted to form arrays of parallel 2D-lines of any orientation. By maintaining a constant L_x/L_y, but varying L_x to give non-commensurate lattice spacings of the HSQ posts (where $L_x \neq L_o$), the PDMS cylinders align themselves diagonally, at different angles along the post lattice. This allows the PDMS cylinders to retain their equilibrium periodicity [81].

In addition, by replacing specific posts with a set of dashes, or closely spaced dots, more complex patterns of PDMS cylinders were produced. The PDMS cylinders align parallel to the dashes and dots, even though these conformations are less favorable than other orientations, based on the larger difference in periodicity between the cylinders. It is assumed that the non-equilibrium formations occur in order to minimize the distortion of the cylindrical PDMS microdomains. By specifying the distribution, shape and angle of the dashes or dots, the PDMS cylinders could be bent by up to 90°, giving bends, jogs and junctions (Fig. 6).

In a similar manner, three-dimensional self-assembled structures were formed on a HSQ post array. The posts were functionalized with a PS brush, resulting in PDMS cylinders forming between the posts. Solvent annealing of the film in a 5:1 volume ratio mixture of toluene and heptane caused the film to swell over the posts, which, once quenched and treated with an O_2 RIE, gave rise to PDMS cylinders in a variety of three-dimensional bilayer lattice structures. By controlling the template arrangement and periodicity, the alignment of the cylinders forming each of the bilayer could be controlled, whilst introducing specific defects into the post array allowed for junctions and bends of desired angles to be fabricated in a predictable manner [82].

Another feature of the PS-*b*-PDMS system is the ability to cross-link the PDMS domains by irradiating the film with an electron-beam, whilst leaving the PS domains unaffected [83]. This preserves the initial morphology of the irradiated block copolymer,

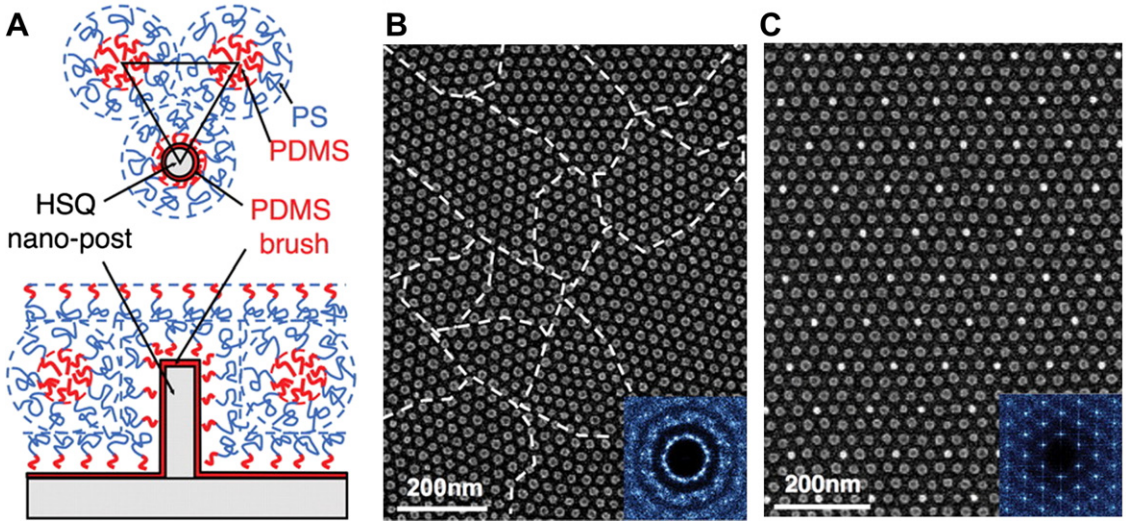

Fig. 5. A – Top-down and side-view schematics showing the arrangement of PS-*b*-PDMS molecules around a single HSQ post, functionalized with a PDMS brush layer. B – SEM image of a PS-*b*-PDMS film with no templating, exposed to an O_2 RIE. Inset shows 2D Fourier transform, indicating absence of long-range order. C – SEM image of a PS-*b*-PDMS film on a HSQ post array template, with substantial long-range ordering of PDMS spheres. Reproduced with permission from Ref. [79].

allowing for a subsequent solvent anneal step, in a different solvent, to change the morphology of the remaining film. Solvent-annealing a PDMS-cylinder forming PS-*b*-PDMS film in acetone gives cylinders of PDMS parallel to the PDMS-brush layer coated Si substrate. Significantly greater swelling of the PS domains occurs when the same polymer film is annealed in N,N-dimethylformamide (DMF), giving spherical PDMS domains. Thus, annealing the polymer film in acetone, followed by electron-beam irradiation of a specified area and a final annealing step in DMF, gives spherical domains of PDMS with cylinders where the film was irradiated (Fig. 7) [84].

Thin films of poly(2-vinylpyridine-*block*-dimethylsiloxane) (P2VP-*b*-PDMS) have also demonstrated great potential for block copolymer lithography. Owing to the extremely high χ-value of the diblock copolymer, fabrication of smaller domains with a smaller period compared to those achieved with PS-*b*-PDMS was demonstrated. The films were annealed with a variety of solvents, and phase-transitions from lamellar, to perforated lamellar, through to cylinders and finally to spheres were demonstrated for the same polymer sample, depending on the swelling ratio (swollen film thickness during solvent anneal/initial thickness) of the polymer domains. Unprecedented control over the thickness of PDMS cylinders parallel to the substrate was also demonstrated. The same sample produced highly-ordered cylinders ranging from 6 to 31 nm in width (a change in volume of 417%), depending on the solvent used for annealing the film and the solvent vapor pressure [85].

2.2. Other Si-containing block copolymers

Whilst PDMS remains the primary choice for silicon-containing BCPs used in block copolymer lithography, it is worthwhile highlighting a few of the alternatives that exist in the literature. This is because, although PS-*b*-PDMS has been shown to be a promising candidate for next-generation BCP lithography masks, preferential wetting of PDMS of both the air/polymer and polymer/substrate interfaces often occurs. This results in the requirement of an additional CF_4 RIE step to remove the air/polymer surface layer, before pattern transfer is possible.

Silsesquioxanes (SSQs) have shown promise as nanolithographic resists. They are a specific type of organosilicate, made up of three silicate linkages per Si, and a final pendant organic substituent – [$RSiO_{1.5}$]. SSQs are synthesized by the hydrolysis of a $RSiX_3$ species (where *X* is an easily hydrolyzed group (e.g. –Cl, alkoxy group (–OR)) and R is an organic substituent stable to hydrolysis) in the presence of an acid or base catalyst. Depending on the nature of the organic substituent, catalyst, temperature and concentration of reagents, SSQs with different architectures may be prepared, with different numbers of cross-linking Si–O–Si moieties. These take the form of random networks, ladders, partial cages, and perfect cages. Perfect cage SSQs offer a material with the high thermal stability, mechanical strength, chemical and physical resistance of an inorganic material, with the solubility and reactivity of an organic material [80,86–88].

Perfect cage SSQ molecules, known as polyhedral oligomeric silsesquioxane (POSS), form semicrystalline or crystalline nanodomains. Upon exposure to an oxygen plasma, POSS is converted to silica, making these materials potential candidates as lithographic resists [89]. The oxygen plasma etch-resistance of the POSS may be incorporated into one block of a phase-separated BCP film, and used to template nanosized features into an underlying substrate.

Initial synthetic routes to POSS-containing BCPs used hydrosilylation reactions to decorate polymers containing pendant unsaturated bonds with POSS units containing a Si–H bond. Polystyrene-*block*-polyisoprene (PS-*b*-PI), was reacted with hydridoheptacyclopentyl substituted POSS, in the presence of Karstedt's catalyst, a soluble platinum complex. A maximum of 92% incorporation of POSS into the polyisoprene units was achieved. Phase-separation of the BCP was observed, but no ordered, continuous domains of PI–POSS were obtained [90].

Through the synthesis of a methacrylate-functionalized POSS (MAPOSS), preparation of BCPs containing POSS were achieved by sequential anionic polymerization (Fig. 8). Bulk films of both PS-*b*-PMAPOSS and PMMA-*b*-PMAPOSS phase-separated, giving spherical, cylindrical and lamellae phases of PMAPOSS, with good long-range order [91,92]. Thin films of both BCPs were spin-coated onto Si wafers, and exposed to an O_2 RIE. The removal of the organic blocks, and conversion of POSS to silica, gave faithful reproduction of the original morphology.

Directed self-assembly of a PMMA-sphere forming PMMA-*b*-PMAPOSS was achieved by spin-coating solutions of the polymer onto a Si wafer with PS brush layer template. The brush layer had been patterned to give a hexagonal array of cross-linked PS spheres, by electron-beam lithography. Annealing the polymer

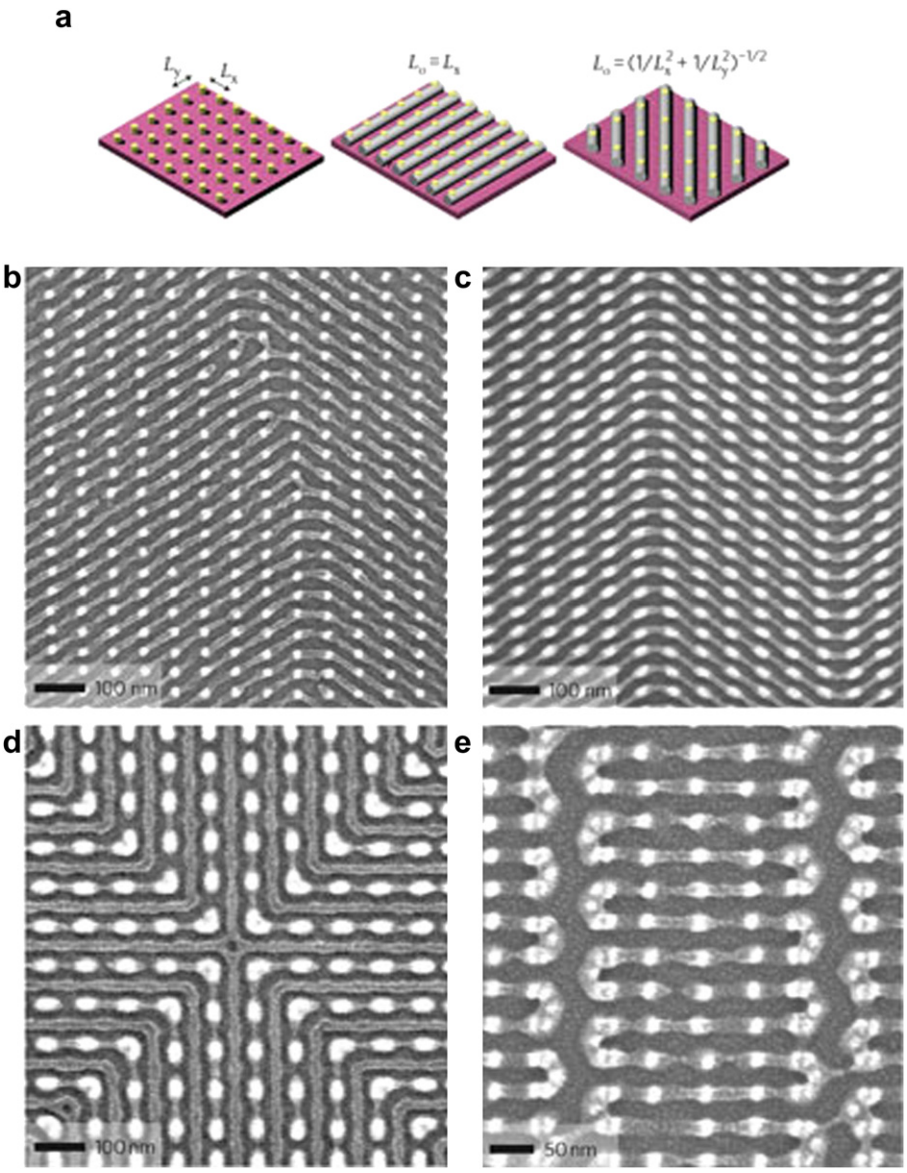

Fig. 6. a) Schematic showing a simplified view of the template consisting of HSQ posts (yellow) on a silicon substrate (pink). b–e) SEM images of PDMS cylinders on HSQ post arrays, forming jogs, bends and junctions. Reproduced with permission from Ref. [81].

film in CS_2 gave highly-ordered, hexagonally-packed PMMA spheres, in a matrix of PMAPOSS, with a 4× density multiplication of the spheres, relative to the underlying brush layer template (Fig. 9) [93].

Early work by Reichmanis and Smolinsky [94] found that the incorporation of >10 wt% of Si into a polymer provides a sufficiently high etch resistance to an oxygen plasma, making it suitable as a pattern transfer mask. Building on this, Yang and co-workers [95] synthesized a range of well-defined, narrowly dispersed Si-containing block copolymers via a nitroxide-mediated radical polymerization route. The styrenic monomers used were 4-(pentamethyldisilyl)-styrene (Si_2St, 24.0 wt% Si), 4-(bis(trimethylsilyl) methyl)styrene (Si_2CSt, 21.4 wt% Si) and 4-(pentamethyldisiloxymethyl)styrene (OSi_2St, 21.2 wt% Si). The bulk film self-assembly of ~75 nm microtomed slices of the BCPs was studied. It was found that the domain size of an 18.2 wt% Si-containing block copolymer, after exposure to an oxygen plasma for 10 min, did not change dramatically, whilst that of a 12.2 wt% Si BCP did, although the polymer film remained intact.

Kim et al. [96] synthesized another Si-containing styrenic monomer, (4-(tert-butyldimethylsilyl)oxystyrene) (SSi, 12 wt% Si). Using this material, they prepared cylinder-forming diblock copolymers of PS-*b*-PSSi, with PSSi as the majority block, via a sequential anionic polymerization route. Thin films of the BCP were spin-coated onto a silicon wafer from 1.5 wt% solutions in xylene. Perpendicular orientation of the PS cylinders was achieved through solvent annealing in a mixed vapor of heptane/toluene 4/1 v/v. These films were treated with an oxygen plasma to remove the PS cylinders and oxidize the PSSi domains, resulting in nanoporous membranes of silicon oxide, with pore sizes of 20, 30 and 50 nm, from three different BCP samples. It was noted that PSSi did not wet the air/polymer interface, eliminating the need for an additional CF_4 RIE step.

Borsali, Ellison, Willson and co-workers paired hydrophilic, rod-like oligosaccharide blocks with a hydrophobic poly(4-trimethylsilylstyrene) (PTMSS) random-coil block, via a copper(I)-catalyzed azide-alkyne cycloaddition "click" route [97]. Three different oligosaccharides were used; linear N-maltoheptaosyl-3-acetamido-1-

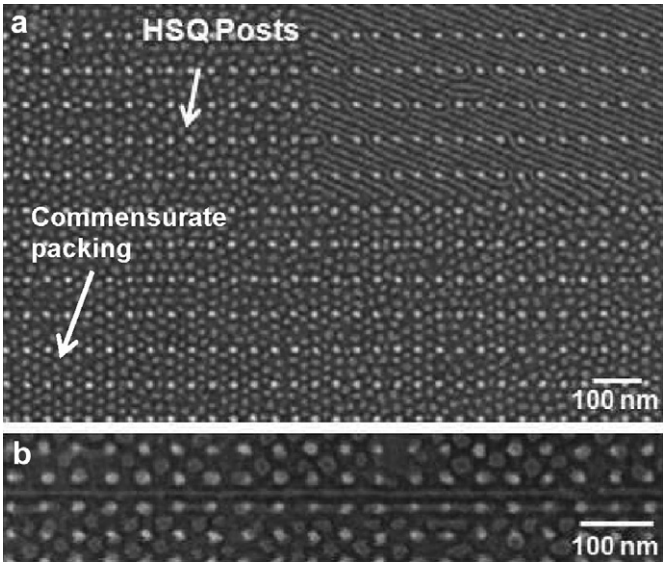

Fig. 7. Dual phase patterns combined with post templating. SEM images of dual phase block copolymer patterns combined with post templates with a period of (a) 45 nm × 78 nm, commensurate with cylinders angled at 23° to the post lattice and a 26 nm center-to-center sphere array aligned along the *y* axis, and (b) 48 nm × 42 nm to form a single line in a square-symmetry sphere array. Reproduced with permission from Ref. [84]. Copyright © 2011, American Chemical Society.

propyne (ethynyl-MH), branched N-xyloglucooligosaccharide-3-acetamido-1-propyne(ethynyl-XGO), and cyclic mono-6A-propargylamino-6A-deoxy-β-cyclodextrin (ethynyl-βCyD). Different molecular weight blocks of PTMSS (PTMSS$_{26}$, M_n = 4.6 kg mol^{-1} and PTMSS$_{15}$, M_n = 2.5 kg mol^{-1}) were prepared via an atom transfer radical polymerization route (ATRP) [98], and both formed the majority blocks of the BCPs. Bulk films were annealed in a 1/1 THF/water mixture to produce hexagonally-packed cylinders for MH-*b*-PTMSS$_{26}$ (domain spacing, d = 10.7 nm, cylinder diameter 5.2 nm), XGO-*b*-PTMSS$_{26}$ (d = 10.1 nm, cylinder diameter 5.1 nm), and MH-*b*-PTMSS$_{15}$ (d = 8.3 nm, cylinder diameter 5.5 nm), as observed by small angle X-ray scattering (SAXS). Perpendicular orientation of cylinders of this size could produce areal feature densities ~8 Tbit/in^2, 8 times that of the current industry target, demonstrating the potential of this particular BCP system. Thin film studies were performed, where a combination of solvent and thermal annealing was employed to manipulate the morphology of the film. Oligosaccharide cylinders parallel to the substrate were obtained, with no PTMSS wetting of the air/polymer interface. The etch selectivity between PTMSS and a mixture of malto-oligosaccharides was calculated to be 28.3, and exposure of a thin film sample of MH-*b*-PTMSS$_{15}$ to an oxygen plasma

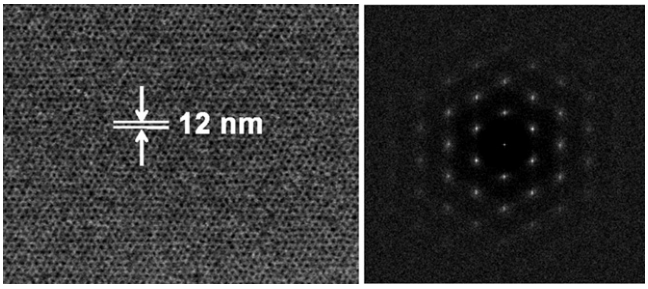

Fig. 9. SEM image and corresponding 2D-FFT image of PMMA$_{25}$-*b*-PMAPOSS$_{13}$ thin films spin-coated onto a Si wafer with EBL patterned PS brush layer. Dark and light regions represent PMMA and PMAPOSS domains, respectively. Reproduced with permission from Ref. [93]. Copyright © 2012, American Chemical Society.

resulted in removal of the oligosaccharide domains, demonstrating the potential of these materials for pattern transfer.

3. Hybrid systems containing inorganic additives

Another way of synthesizing an inorganic BCP is by selectively introducing an inorganic additive into one segment of an organic BCP. This results in an increase in the etch selectivity of the material which allows for greater efficiency of pattern transfer of the desired microphase into the underlying substrate, relative to organic BCPs.

The block copolymer, polystyrene-*block*-poly(ethylene oxide) (PS-*b*-PEO), has been studied extensively by Kim et al. as an inorganic support matrix, owing to the selective miscibility of oligomeric organosilicates (OS) within the PEO domains. Binary solutions of PS-*b*-PEO and OS were spin-coated onto a substrate, giving films of the desired thickness. The films were subsequently baked at 450 °C. This cross-links the organosilicate (150 °C) within the PEO domains, and causes the thermal decomposition of the PS-*b*-PEO matrix (450 °C). The structure of the PEO + OS domain is preserved and can then be used to pattern the underlying substrate (Fig. 10) [99,100].

Further work utilized graphoepitaxial directed self-assembly to give improved long-range order in the system. Generally, trenches of targeted periodicity and height were etched into either a poly(-methyl methacrylate) (PMMA) or hydrogen silsesquioxane (HSQ) resist substrate with an e-beam, and subsequent lift-off process. Sputtering of the desired substrate material onto the patterned resist gave the topographically patterned substrate. Finally, the pre-treatment of the bottom of the trenches with a variety of materials gave a neutral surface for both the PS and PEO + OS domains [101,102].

The nature of the organosilicate has been also been studied. It was found that greater long-range order in the self-assembled films

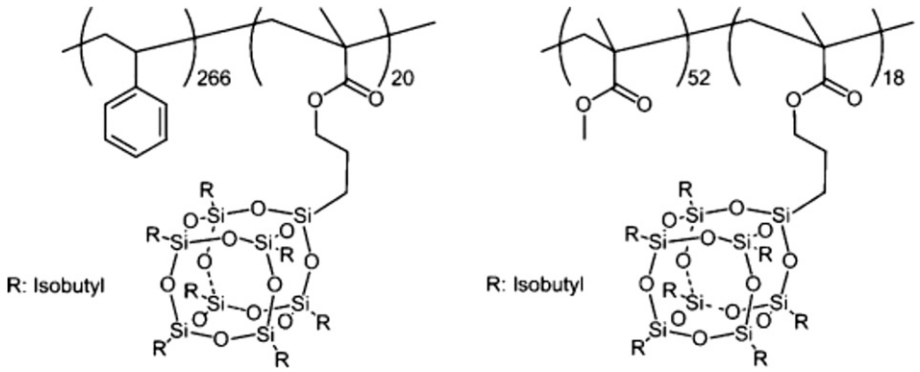

Fig. 8. Structural representations of PS-*b*-PMAPOSS (left) and PMMA-*b*-PMAPOSS (right). Reproduced with permission from Ref. [92].

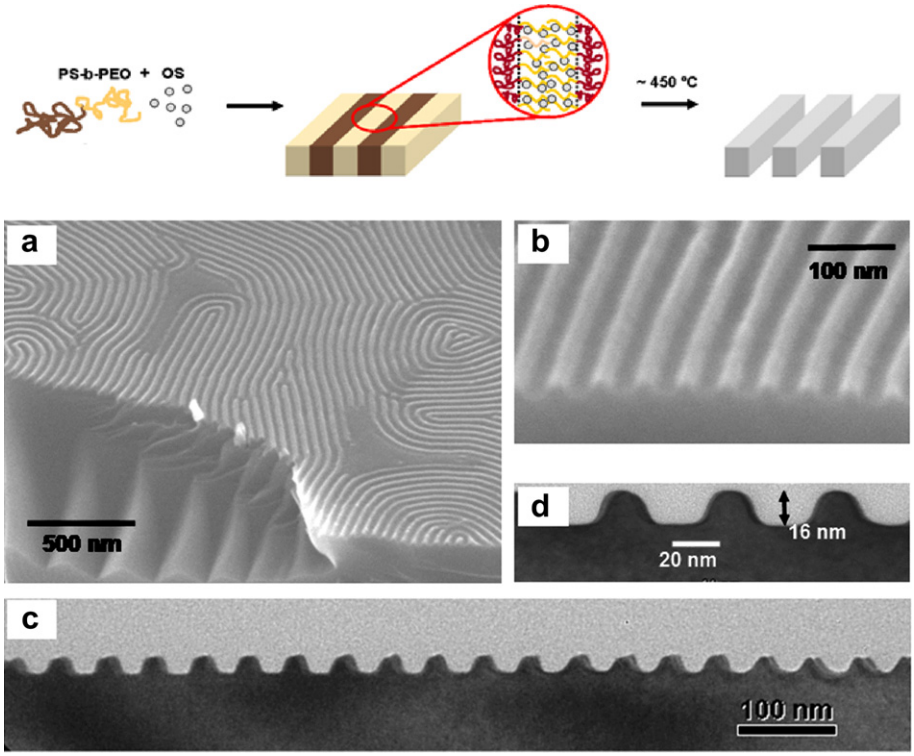

Fig. 10. Top – Schematic representation of line patterns from the lamellar phase of PS-*b*-PEO/OS hybrid. Bottom – Electron micrographs of the silicon surface after transferring self-assembled OS lamellae shown. The OS patterns were transferred by 30 s CF_4 plasma etching followed by 5 wt% HF rinsing. (a) Low magnification SEM image. (b) High magnification SEM image. [(c) and (d)] High resolution cross-sectional TEM images of the silicon wafer. Reproduced with permission from Refs. [100,102].

was obtained with lower molecular weight copolymers of methyltrimethoxysilane (MTMOS) and tetraethoxysilane (TEOS), containing a greater ratio of MTMOS to TEOS [103]. By varying the amount of OS added to the PS-*b*-PEO, the volume fraction of the PEO + OS domain can be selectively tuned, giving a great degree of flexibility over the desired morphology of the hybrid diblock copolymer [101]. This is advantageous over traditional block copolymer systems, where it is necessary to synthesize individual block copolymers of specific volume fractions to give the desired morphology. In addition, the increase in Flory-Huggins interaction parameter between the PS and PEO coblocks allows for the preparation of low molecular weight polymers which still phase-separate, giving smaller nanodomains with a reduced period. For example, 7 nm half-pitch line patterns have been demonstrated using a low molecular weight PS-*b*-PEO (5.1 kg mol^{-1}, PS = 3 kg mol^{-1}, PEO = 2.1 kg mol^{-1}) blended with OS [102].

The hybrid PS-*b*-PEO/OS system has also used as a template to pattern single and multilayer antidot arrays in Co and Co/Cu/NiFe films. Antiparallel alignment of the magnetic moments was observed in multilayer films, in the Co and NiFe layers at

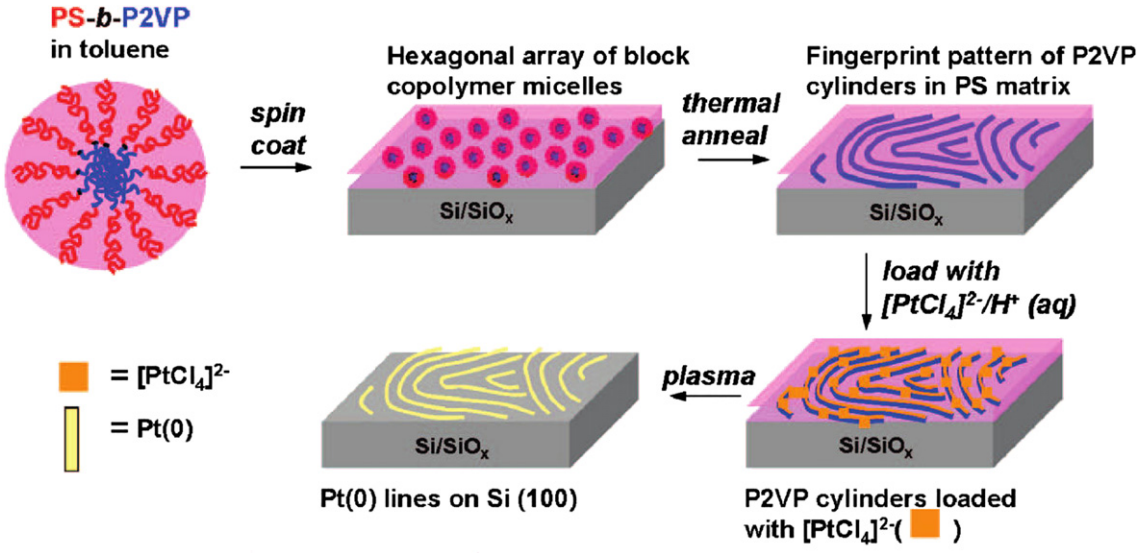

Fig 11. Schematic representation of parallel platinum lines on a Si wafer, prepared from a micellular solution of PS-*b*-P2VP, loaded with $[PtCl_4]^{2-}$. Reproduced with permission from Ref. [127]. Copyright © 2008, American Chemical Society.

remanence, due to strong magnetostatic interactions between the layers. In addition, the 20 nm antidot Co monolayer raised the coercivity with respect to those of continuous Co monolayer films [104]. The same polymer, producing an antidot morphology was used in a bilayer approach to produce a nanoporous template with pores orientated perpendicular to the substrate. The nanopores were filled with a titania precursor by thermal infiltration, and then baked, leaving free-standing titania nanoposts [105].

In a similar approach, titania nanodot arrays have been prepared, using a PS-*b*-PEO + titania precursor (titanium tetraisopropoxide) [106]. Immersion of cylinder-forming films of PS-*b*-PEO in water swells the PEO domains. Subsequent exposure of the films to vapors of $SiCl_4$ or $TiCl_4$, led to silica or titania dot arrays at the polymer/vapor interface [107]. Nanoscopic silica posts have been grown using perpendicular cylinder-forming polystyrene-*block*-poly(methyl methacrylate) (PS-*b*-PMMA) films. The films were irradiated with UV light, removing the PMMA cylinders and cross-linking the PS matrix. After an acetic acid wash, the porous PS film was exposed to $SiCl_4$ vapors, where silica growth was stimulated by the reaction of $SiCl_4$ with trace amounts of water, with growth propagating from the condensation onto the silanol groups protruding from the silica surface in the bottom of the pores. A final CF_4 RIE etch revealed silica nanoposts [108]. Selective mineralization of silica and alumina within the PMMA cylinders of a PS-*b*-PMMA block copolymer, using the relevant inorganic precursor, has also been demonstrated [109,110].

In addition to the fabrication of well-ordered, nanoscale, semiconducting materials for integrated circuits, the semiconductor industry also requires the fabrication of metal nanostructures, whether to function as interconnects or as active components themselves [111–118]. This can be achieved through the introduction of a metal-containing species into one block of a phase-separated, all-organic block copolymer, followed by selective etching of the remaining coblock. *Ex situ* methods, involving the surface-functionalization of metallic nanoparticles, enabling their selective solvation in a particular block of a block copolymer, have been demonstrated [119–122]. *In situ* methods, generally involving the reduction of selectively impregnated metal ions to metal nanoparticles, have also been described [123–125]. However, the majority of these methods involve the formation of spherical metal nanoparticles embedded in a selected block, not continuous metallic domains, which are essential for good electrical conductivity.

Buriak and co-workers have developed an *in situ* method for the fabrication of highly-ordered, nanoscale metallic features. Polystyrene-*block*-poly(2-vinylpyridine) (PS-*b*-P2VP) films were

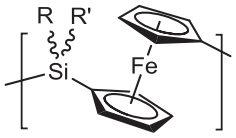

Fig. 13. Structure of PFS.

impregnated with metal ions from an acidic anionic metal solution [126]. Solutions of PS-*b*-P2VP in toluene were spin-coated onto a Si wafer with a native oxide layer, and the films were then thermally annealed to produce parallel P2VP cylinders with a period of 36 nm in a PS matrix. Immersion of the film into, for example, a 10 mM solution of $Na_2[PtCl_4]$ (aq) containing 0.9% HCl (aq), for 3 h, followed by a 30 s O_2 RIE, gave platinum lines on the silicon surface. A schematic representation is shown in Fig. 11. The thickness of the platinum lines could be controlled by changing the concentration of the acidic platinum solution. Nanowires with a diameter of ~7.2 nm and height of ~9.2 nm were obtained from a 0.1 mM solution. Increasing the concentration to 1 mM and 10 mM gave dimensions of 9.6 × 11.6 nm and 11.6 × 13.5 nm, respectively. This increase in size was accompanied by a loss in resistance per unit length, from 3.0 kΩ nm^{-1} to 1.9 kΩ nm^{-1} and 1.2 kΩ nm^{-1}. The wires exhibited ohmic conduction, although the electrical resistivity of the Pt nanowires (~1.0×10^{-4} Ωm) was found to be higher than that of bulk platinum (1.1×10^{-7} Ωm).

The technique described relies on the swelling of the P2VP phase upon protonation [128,129]. Aqueous H^+ ions diffuse through the PS matrix, which preferentially forms at the air/polymer interface of the film. The swollen P2VP phase erupts through the PS matrix at the air/polymer interface, forming "mushroom caps". The cationic P2VP chains were exposed to the anionic $[PtCl_4]^{2-}$ (aq), leading to electrostatic binding of the two species. In this sense, the system was further expanded, with the fabrication of continuous gold (10 mM $HAuCl_4$/0.9% HCl (aq), 3 h immersion), palladium (10 mM $Na_2[PdCl_4]$/0.9% HCl (aq), 3 h immersion), iron (10 mM $K_3Fe(CN)_6$/0.9% HCl (aq), 3 h immersion), cobalt (10 mM $K_3Co(CN)_6$/0.9% HCl (aq), 3 h immersion), copper (10 mM $CuCl_2$/0.9% HF (aq), 15 min immersion) and nickel (10 mM $NiCl_2$/0.9% HF (aq), 15 min immersion) features. Binding of cationic metallic species, such as $[Ag(H_2O)_6]^+$ (from aqueous $AgNO_3$) was unsuccessful, due to the net repulsion with the cationic protonated P2VP chains [127].

Electron-beam lithography was used to pattern features in the substrate for directed self-assembly. Formation of both well-

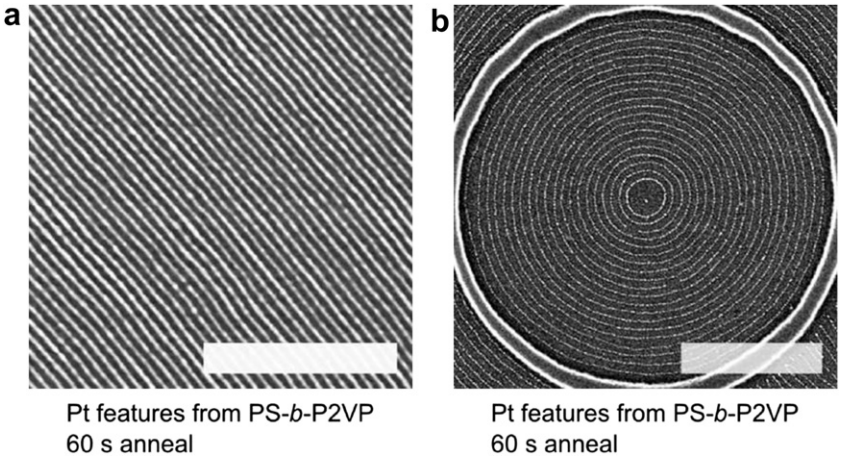

Fig. 12. SEM images of Pt lines templated from PS-*b*-P2VP. Samples were microwave annealed for 60 s at 130 °C in the presence of THF. a) No graphoepitaxial patterning, b) circular SiO_2 feature for graphoepitaxy. Scale bar represents 500 nm. Reproduced with permission from Ref. [130]. Copyright © 2010, American Chemical Society.

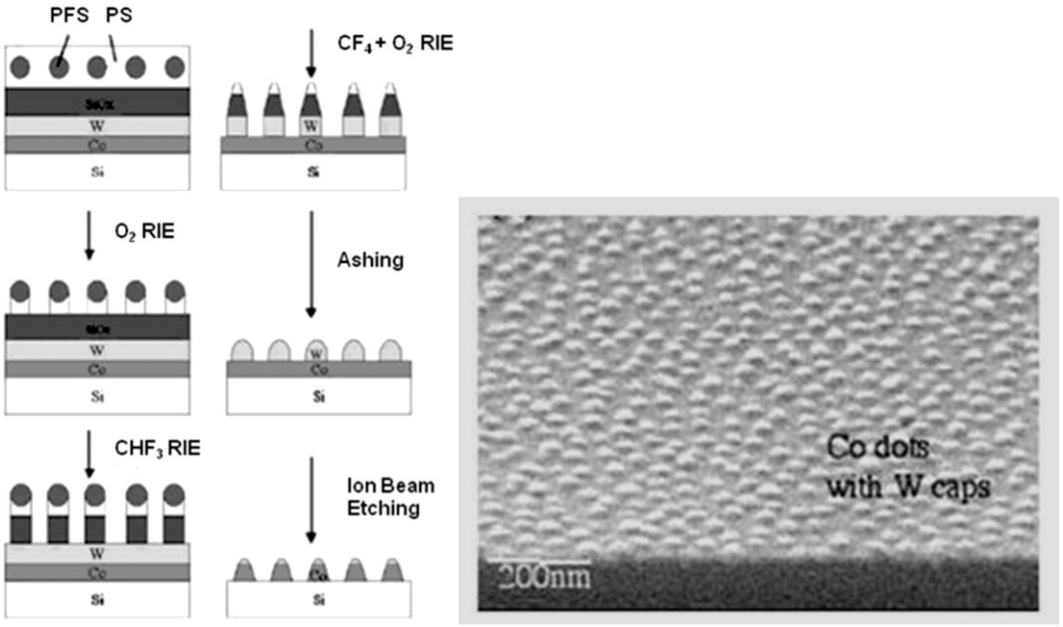

Fig. 14. Fabrication of cobalt nanodot arrays using PS-*b*-PFS thin film block copolymer lithography. Reproduced with permission from Ref. [36].

ordered concentric rings in circular trenches, and parallel lamellae in straight trenches was achieved. Further work demonstrated the use of a commercial microwave reactor to achieve highly-ordered P2VP cylinders, parallel to the graphoepitaxially patterned substrate, with as little as 60 s annealing at 120 °C, as shown in Fig. 12 [130]. This is of great importance when considering the processes' applicability for commercialization. Highly-ordered nanowires with a defect density of 2 defects/μm^2 were obtained from films of $PS_{32.5}$-*b*-$P2VP_{12}$ (subscript denotes molar mass of block, kg mol^{-1}) after 180 s of microwave and thermal annealing. Reproducible density doubling of P2VP cylinders or spheres, through careful manipulation of the initial film thickness and solvent annealing conditions, has also been shown [131]. Highly-ordered nanowires with periods ranging from 17 nm ($PS_{23.6}$-*b*-$P2VP_{10.4}$) to 41 nm (PS_{125}-*b*-$P2VP_{58.5}$) were obtained.

4. Poly(ferrocenylsilane)-containing block copolymers

Polyferrocenylsilanes (PFSs) are metal-containing polymers with iron and silicon in the polymer backbone (Fig. 13) [132,133]. The presence of iron in the main chain means PFSs possess a number of interesting properties, including resistance to reactive ion etching. On exposure to an oxygen plasma, PFS thin films have been shown by Vancso and Thomas to act as an etch barrier, forming an iron/silicon oxide layer at the film's surface as established by X-ray photoelectron spectroscopy [134,135]. This is in contrast to most organic polymers where volatile compounds are formed and removed from the surface. PFS-containing BCPs, where the selective removal of organic coblocks by RIE can be achieved, have therefore been utilized in the fabrication of nanoscale domains by nanolithographic applications [136–139].

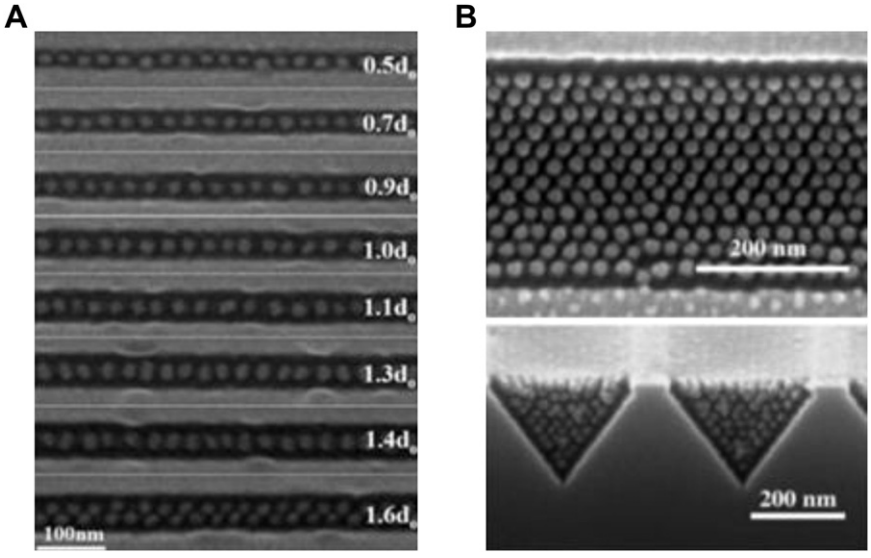

Fig. 15. SEM images of PS-*b*-PFS thin films, following O_2 etching, confined in A) channels of different confinement widths, B) and in V-shaped grooves, which induce a fcc packing arrangement (reproduced with permission from Refs. [141,142]). Copyright © 2006, American Chemical Society.

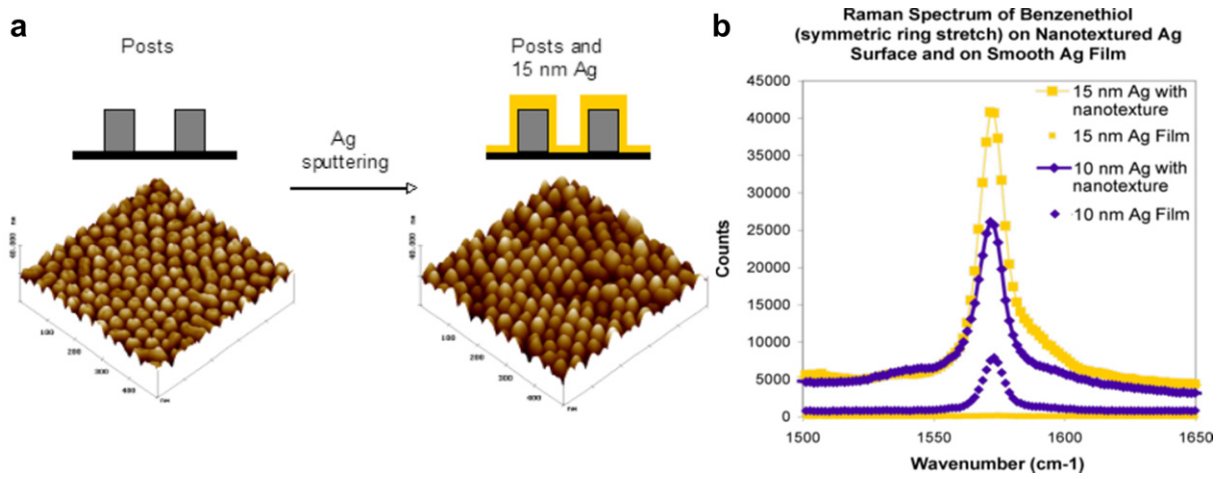

Fig. 16. Generation of a silver nanotextured surface for SERS using a PS-*b*-PFS diblock copolymer thin film. AFM height images (left) of PFS posts following UV-ozone etched of a PS-*b*-PFS thin film and nanotextured silver surface (right) from sputtering (a). Surface enhanced Raman spectra (b) of benzenethiol on nanotextured Ag films (10 and 15 nm: ◆ and ■ respectively) and control experiments with smooth Ag films (10 and 15 nm: -◆- and -■- respectively). (Adapted from Ref. [144]).

For example, Ross and co-workers have prepared arrays of single-domain cobalt nanodots using a polystyrene-*block*-poly(ferrocenylsilane) (PS-*b*-PFS, $\chi = 0.08$ [140]) diblock copolymer thin film as a template [36]. The first step involved spin-coating the PS-*b*-PFS copolymer on to a silica substrate, followed by the removal of the PS matrix to reveal PFS spherical domains using an O_2 RIE. Direct pattern transfer to an underlying tungsten layer was the achieved by successive etching using $CF_4 + O_2$ RIE and ashing. Finally, an ion beam etch was used to form tungsten-capped cobalt dots with pattern and dimensions inherited from the original PS-*b*-PFS film (Fig. 14).

Using a similar PS-*b*-PFS diblock copolymer, isolated 1D arrays of PFS spheres were produced, by confining PS-*b*-PFS diblock copolymer thin films in etched channels 30–80 nm in width [141]. When the channel width was equal to the row spacing, single rows of PFS spheres were formed. However, as the groove width increased and became incommensurate with the period of the BCP, the domains become distorted, and elliptical in shape. When the channel became wide enough to accommodate a second row of spheres the distortion is removed (Fig. 15A). In addition, the influence of topographically patterned substrates on the morphology and close packing of PS-*b*-PFS was also studied by templating thin films within V-shaped groves [142]. Without confinement, body-centred cubic (bcc) packing is the equilibrium state for spherical morphologies, however templating in the V-shaped groves promoted a face-centred cubic (fcc) packing (Fig. 15B). Insightful studies of the topographic ordering of other block copolymers such as PI-*b*-PFS have also been reported [143].

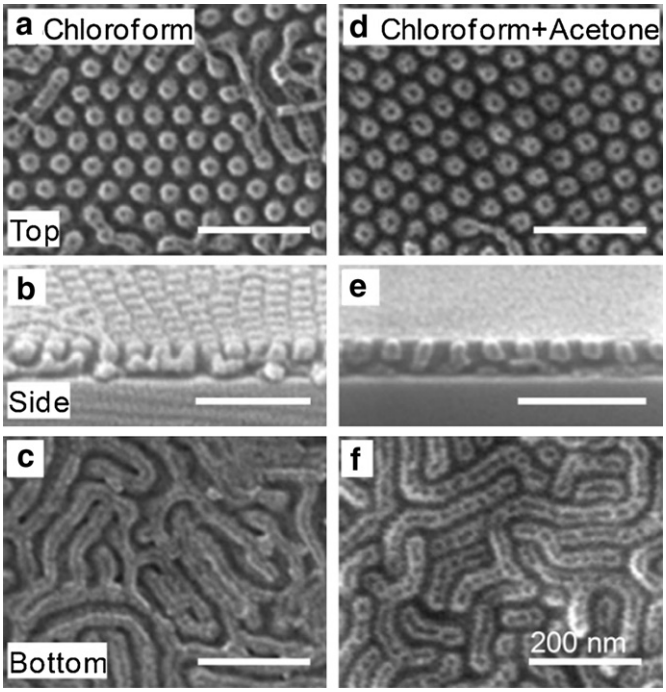

Fig. 17. SEM images of thin films of PS-*b*-PFS-*b*-P2VP after annealing in (a)–(c) chloroform and (d)–(f) a mixed solvent vapor of chloroform and acetone for 4 h at room temperature, followed by etching with oxygen RIE. (a), (d) Plane-view, (b), (e) side-view, (c), (f) bottom-view (reproduced with permission from Ref. [145]).

A silver nanotextured surface, prepared by sputtering silver onto PFS cylinders generated from a PS-*b*-PFS thin film, has been used as a substrate for Surface Enhanced Raman Spectroscopy (SERS) (Fig. 16) [144]. Amplified Raman signals were observed for absorbed benzenethiol, with enhancement factors up to 10^6.

Nanoscale ring arrays have been prepared from a polystyrene-*block*-polyferrocenylsilane-*block*-poly(2-vinylpyridine) (PS-*b*-PFS-*b*-P2VP) triblock terpolymer [145]. Such ring-shaped structures have potential applications in the fabrication of memories or sensors [69,73,146] and quantum devices [147–149]. Thin film self-assembly of the PS-*b*-PFS-*b*-P2VP triblock terpolymer gave a core/shell cylinder morphology of 50 nm period consisting of a PS core with PFS shell in a P2VP matrix perpendicular to the film surface. The PS and P2VP domains were selectively removed by exposure to an oxygen plasma, leaving partly oxidized PFS rings 33 nm in diameter and 11 nm wide. The presence of two organic (PS and P2VP) blocks and an organometallic (PFS) block results in high etch selectivity due to the resistance of PFS to oxygen plasma and enhanced pattern transfer compared to all-organic triblock terpolymers. As the PFS cylinders did not span the entire film thickness, the ring patterns were transferred into a PS layer by imprinting (Fig. 17).

Using a similar approach, thin films of a polyisoprene-*block*-polystyrene-*block*-polyferrocenylsilane triblock terpolymer and a PI-*b*-PS-*b*-PFS/PS homopolymer blend have been used to prepare nanoscale square-symmetry arrays [150]. Access to such geometries is very difficult using the self-assembly of diblock copolymers, yet it is a device geometry considered essential for future lithography needs, for example as via array structures in integrated circuits [39]. Square-packed PI and PFS cylinders in a PS matrix were formed in thin films of the PI-*b*-PS-*b*-PFS triblock terpolymer and PI-*b*-PS-*b*-PFS/PS blend. Ordering was improved by addition of the PS homopolymer, which is thought to stabilize the square-packed morphology by occupying volume between the cylinders allowing the highly stretched triblock terpolymer chains to relax. The organic blocks were again removed via an O_2 RIE step to expose square-packed PFS cylinders with a 40.5 nm period which extended throughout the film thickness. Pattern transfer of the PFS domains to a 30 nm thick silica film by successive etching gave a square array of silica posts of 20 nm diameter and 30 nm height.

The thin film self-assembly of the PI-*b*-PS-*b*-PFS/PS blend was also templated on topographical substrates with shallow groves etched into the silicon. The periodicity of the templated square arrays could be varied with trench width and orientation of the PFS domains controlled by treating the substrate with a PS brush. Preferential wetting of the middle PS block to the trench wall changes the lattice vector of the PFS array from 90° to 45° with respect to the trench edge. In thicker films, in-plane cylinders were obtained where the orientation of the cylinders with respect to the trench wall could again be controlled by treating the substrate with a PS brush. In addition, it has been demonstrated that the grain size of the square-packed PFS domains can be increased up to several micrometers using templates consisting of topographical posts and rectangular walls (Fig. 18) [151].

Further studies on the same PI-*b*-PS-*b*-PFS/PS polymer blend have shown surface reconstruction of the thin films to be possible [152]. Immersion of the films into liquid hexane, a selective solvent for PI, draws the PI cylinders to the air/polymer surface. After rapid quenching with a stream of nitrogen gas a square-packed hole array is obtained, which can subsequently be transferred into a silicon substrate via wet and dry etching methods. The diameter of the holes can be widened from 15 nm to 21 nm and 30 nm by

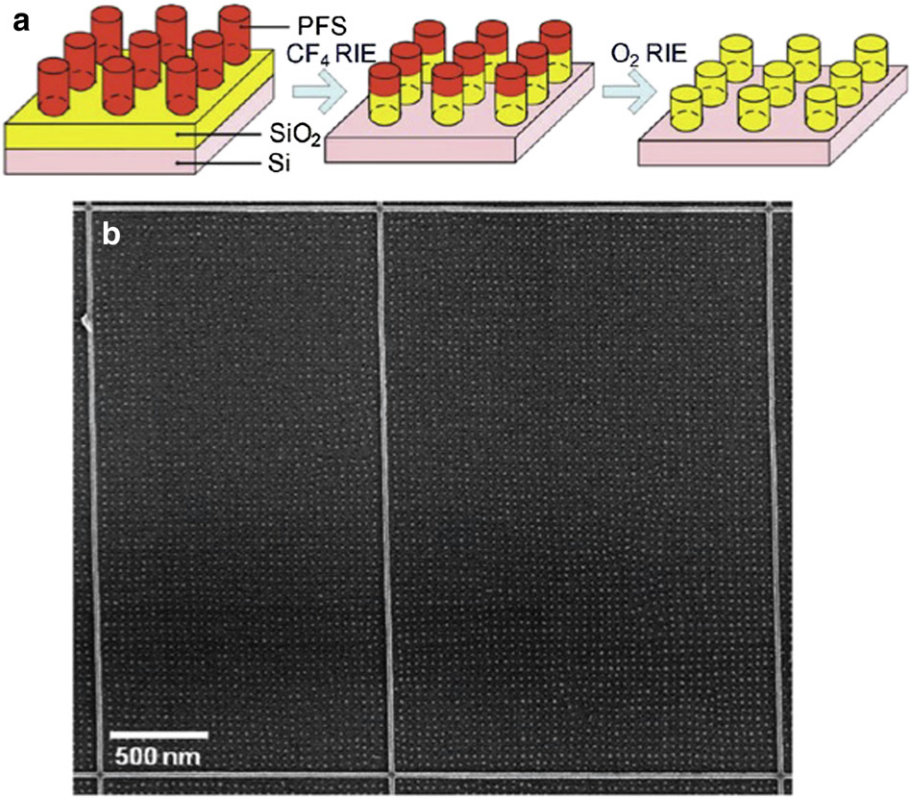

Fig. 18. Pattern transfer to form square arrays of silica posts from PI-*b*-PS-*b*-PFS. (a) Schematic of the pattern transfer process. (b) SEM image showing highly-ordered square arrays of oxidized PFS microdomains templated with HSQ sidewalls. Reproduced with permission from Ref. [150,151]. Copyright © 2011, American Chemical Society.

subjecting the film to an oxygen RIE for 10 s and 15 s, respectively. Exposures exceeding 30 s completely remove both the PI and PS domains, revealing a square-packed array of oxidized PFS cylinders. This study illustrates the flexibility of triblock terpolymer systems to fabricate multiple patterns from a single material.

In a different approach, cylindrical micelles derived from the self-assembly of PFS-*b*-PDMS and PI-*b*-PFS in selective solvents for the PDMS and PI blocks have also shown interesting potential in nanolithography. Si wafers were either spin- or dip-coated with micelle solutions, and subsequently etched with an O_2 plasma. This resulted in continuous ceramic nanolines, with variable width from 8 nm (PI-*b*-PFS) to 30 nm (PFS-*b*-PDMS), depending on the composition of micelle corona [153].

Thin films of PS-*b*-PFS block copolymers have also been shown to function as precursors to nanostructured magnetic nanodomains [154] and the possibility for direct nanopatterning of magnetic materials using a combined lithography/thermal treatment approach offers interesting future opportunities.

5. Summary and outlook

Block copolymer lithography shows great potential as an emerging technology for nanoscale device fabrication. Conveniently, block copolymer lithography is largely compatible with current manufacturing processes used in the semiconductor industry and offers a low cost alternative to photolithography for pattern transfer. Essential to the realization of this technology is a combination of control over the long-range ordering of the BCP domains, efficient pattern transfer of BCP film features into underlying substrates, and scalability of the pattern features to sub-10 nm. This review has illustrated that the introduction of inorganic segments into organic block copolymers increases both χ and the etch selectivity of the blocks, enabling these conditions to be met. Inorganic blocks also provide an opportunity to directly pattern functional materials such as metals or magnetic materials.

Acknowledgements

A.N. would like to thank EPSRC and NSF for financial support. In addition, J.G. would like to the EU for financial support. I.M. thanks the European Union for an Advanced Investigator Grant and also the Royal Society for a Wolfson Research Merit Award. In addition, we'd like to thank Prof. Caroline Ross for valuable input and Prof. Paul Rupar for the TOC abstract design.

References

[1] Moore GE. Proceedings of SPIE 1995;2437:2–17.
[2] Kusumoto S, Shima M, Wang Y, Shimokawa T, Sato H, Hieda K. Polymers for Advanced Technologies 2006;17(2):122–30.
[3] Hori M, Nagai T, Nakamura A, Abe T, Wakamatsu G, Kakizawa T, et al. Sub-40nm half-pitch double patterning with resist freezing process – art. no. 69230H. In: Henderson CL, editor. Advances in resist materials and processing technology XXV, Pts 1 and 2, vol. 6923. Bellingham: SPIE – Int Soc Optical Engineering; 2008. p. H9230.
[4] Luttge R. Journal of Physics D – Applied Physics 2009;42(12):123001.
[5] Mack C. Fundamental principles of optical lithography: the science of microfabrication. John Wiley & Sons; 2008.
[6] Lu W, Sastry AM. IEEE Transactions on Semiconductor Manufacturing 2007; 20(4):421–31.
[7] Acikgoz C, Hempenius MA, Huskens J, Vancso GJ. European Polymer Journal 2011;47(11):2033–52.
[8] Tseng AA, Chen K, Chen CD, Ma KJ. IEEE Transactions on Electronics Packaging Manufacturing 2003;26(2):141–9.
[9] Melngailis J, Mondelli AA, Berry III IL, Mohondro R. Journal of Vacuum Science & Technology B: Microelectronics and Nanometer Structures 1998; 16(3):927–57.
[10] Vladimirsky Y, Bourdillon A, Vladimirsky O, Jiang W, Leonard Q. Journal of Physics D – Applied Physics 1999;32(22):L114–8.
[11] Guo LJ. Journal of Physics D – Applied Physics 2004;37(11):R123–41.
[12] Nedoma AJ, Robertson ML, Wanakule NS, Balsara NP. Macromolecules 2008; 41(15):5773–9.
[13] Lee JH, Balsara NP, Chakraborty AK, Krishnamoorti R, Hammouda B. Macromolecules 2002;35(20):7748–57.
[14] Lefebvre AA, Balsara NP, Lee JH, Vaidyanathan C. Macromolecules 2002; 35(20):7758–64.
[15] Zirkel A, Gruner SM, Urban V, Thiyagarajan P. Macromolecules 2002;35(19): 7375–86.
[16] Ryu DY, Jeong U, Lee DH, Kim J, Youn HS, Kim JK. Macromolecules 2003; 36(8):2894–902.
[17] Elbs H, Krausch G. Polymer 2004;45(23):7935–42.
[18] Sun Z, Wang CH. Journal of Chemical Physics 1995;103(9):3762–6.
[19] Posharnowa N, Schneider A, Wünsch M, Kuleznew V, Wolf BA. Journal of Chemical Physics 2001;115(20):9536–46.
[20] Fukuda T, Nagata M, Inagaki H. Macromolecules 1984;17(4):548–53.
[21] Marsac P, Li T, Taylor L. Pharmaceutical Research 2009;26(1):139–51.
[22] Matsen MW, Schick M. Physical Review Letters 1994;72(16):2660–3.
[23] Bates FS, Fredrickson GH. Annual Review of Physical Chemistry 1990;41: 525–57.
[24] Gokan H, Esho S, Ohnishi Y. Journal of the Electrochemical Society 1983; 130(1):143–6.
[25] Harrison C, Park M, Chaikin PM, Register RA, Adamson DH. Journal of Vacuum Science & Technology B 1998;16(2):544–52.
[26] Guarini KW, Black CT, Yeung SHI. Advanced Materials 2002;14(18): 1290–4.
[27] Zschech D, Kim DH, Milenin AP, Scholz R, Hillebrand R, Hawker CJ, et al. Nano Letters 2007;7(6):1516–20.
[28] Mansky P, Harrison CK, Chaikin PM, Register RA, Yao N. Applied Physics Letters 1996;68(18):2586–8.
[29] Park M, Harrison C, Chaikin PM, Register RA, Adamson DH. Science 1997; 276(5317):1401–4.
[30] Nitta S, Ponoth S, Brera G, Coibum M, Clevenger L, Horak D, et al. A multilevel copper/low-k/airgap BEOL technology. In: McKerrow AJ, ShachamDiamand Y, Shingubara S, Shimogaki Y, editors. Advanced Metallization Conference 2007, vol. 23. Warrendale: Materials Research Society; 2008. p. 329–36.
[31] Black CT, Guarini KW, Milkove KR, Baker SM, Russell TP, Tuominen MT. Applied Physics Letters 2001;79(3):409–11.
[32] Black CT, Guarini KW, Zhang Y, Kim HJ, Benedict J, Sikorski E, et al. IEEE Electron Device Letters 2004;25(9):622–4.
[33] Black CT. Applied Physics Letters 2005;87(16):3.
[34] Black CT, Ruiz R, Breyta G, Cheng JY, Colburn ME, Guarini KW, et al. IBM Journal of Research and Development 2007;51(5):605–33.
[35] Guarini KW, Black CT, Zhang Y, Babich IV, Sikorski EM, Gignac LM, et al. Low voltage, scalable nanocrystal FLASH memory fabricated by templated self assembly. New York: IEEE; 2003.
[36] Cheng JY, Ross CA, Chan VZH, Thomas EL, Lammertink RGH, Vancso GJ. Advanced Materials 2001;13(15):1174–8.
[37] Hamley IW. Progress in Polymer Science 2009;34(11):1161–210.
[38] Stoykovich MP, Kang H, Daoulas KC, Liu G, Liu CC, de Pablo JJ, et al. ACS Nano 2007;1(3):168–75.
[39] Tang CB, Lennon EM, Fredrickson GH, Kramer EJ, Hawker CJ. Science 2008; 322(5900):429–32.
[40] Park S, Lee DH, Xu J, Kim B, Hong SW, Jeong U, et al. Science 2009;323(5917): 1030–3.
[41] Hawker CJ, Russell TP. MRS Bulletin 2005;30(12):952–66.
[42] Segalman RA. Materials Science & Engineering R – Reports 2005;48(6):191–226.
[43] Cheng JY, Ross CA, Smith HI, Thomas EL. Advanced Materials 2006;18(19): 2505–21.
[44] Kim HC, Park SM, Hinsberg WD. Chemical Reviews 2010;110(1):146–77.
[45] Park C, Yoon J, Thomas EL. Polymer 2003;44(22):6725–60.
[46] O'Driscoll S, Demirel G, Farrell RA, Fitzgerald TG, O'Mahony C, Holmes JD, et al. Polymers for Advanced Technologies 2011;22(6):915–23.
[47] Shin DO, Lee DH, Moon HS, Jeong SJ, Kim JY, Mun JH, et al. Advanced Functional Materials 2011;21(2):250–4.
[48] Hong SW, Huh J, Gu XD, Lee DH, Jo WH, Park S, et al. Proceedings of the National Academy of Sciences of the United States of America 2012;109(5): 1402–6.
[49] Russell TP, Hjelm RP, Seeger PA. Macromolecules 1990;23(3):890–3.
[50] Nose T. Polymer 1995;36(11):2243–8.
[51] Lindvig T, Michelsen ML, Kontogeorgis GM. Fluid Phase Equilibria 2002; 203(1–2):247–60.
[52] Wang Q, Yang JH, Yao WW, Wang K, Du RN, Zhang Q, et al. Applied Surface Science 2010;256(20):5843–8.
[53] Yang JH, Wang Q, Yao WW, Chen F, Fu QA. Applied Surface Science 2011; 257(11):4928–34.
[54] Zhang S, Hou Z, Gonsalves KE. Journal of Polymer Science Part A – Polymer Chemistry 1996;34(13):2737–42.
[55] Rodwogin MD, Spanjers CS, Leighton C, Hillmyer MA. ACS Nano 2010;4(2): 725–32.
[56] Voet VSD, Pick TE, Park SM, Moritz M, Hammack AT, Urban JJ, et al. Journal of the American Chemical Society 2011;133(9):2812–5.
[57] Guo LJ. Advanced Materials 2007;19(4):495–513.
[58] Park SM, Liang XG, Harteneck BD, Pick TE, Hiroshiba N, Wu Y, et al. ACS Nano 2011;5(11):8523–31.

[59] Lee MJ, Lee NY, Lim JR, Kim JB, Kim M, Baik HK, et al. Advanced Materials 2006;18(23):3115–9.
[60] Newby BMZ, Chaudhury MK, Brown HR. Science 1995;269(5229): 1407–9.
[61] Thanawala SK, Chaudhury MK. Langmuir 2000;16(3):1256–60.
[62] Chao CC, Ho RM, Georgopanos P, Avgeropoulos A, Thomas EL. Soft Matter 2010;6(15):3582–7.
[63] Zhu JG, Zheng YF, Prinz GA. Journal of Applied Physics 2000;87(9): 6668–73.
[64] Chao CC, Wang TC, Ho RM, Georgopanos P, Avgeropoulos A, Thomas EL. ACS Nano 2010;4(4):2088–94.
[65] Jung YS, Ross CA. Nano Letters 2007;7(7):2046–50.
[66] Andersen TH, Tougaard S, Larsen NB, Almdal K, Johannsen I. Journal of Electron Spectroscopy and Related Phenomena 2001;121(1–3):93–110.
[67] Jung YS, Jung W, Tuller HL, Ross CA. Nano Letters 2008;8(11):3776–80.
[68] Jung YS, Jung W, Ross CA. Nano Letters 2008;8(9):2975–81.
[69] Castaño FJ, Morecroft D, Jung W, Ross CA. Physical Review Letters 2005; 95(13):137201.
[70] Hill MT, Dorren HJS, de Vries T, Leijtens XJM, den Besten JH, Smalbrugge B, et al. Nature 2004;432(7014):206–9.
[71] Llandro J, Hayward TJ, Morecroft D, Bland JAC, Castaño FJ, Colin IA, et al. Applied Physics Letters 2007;91(20):203904.
[72] Matveev KA, Larkin AI, Glazman LI. Physical Review Letters 2002;89(20): 096802.
[73] Miller MM, Prinz GA, Cheng SF, Bounnak S. Applied Physics Letters 2002; 81(12):2211–3.
[74] Pauzauskie PJ, Sirbuly DJ, Yang P. Physical Review Letters 2006;96(14): 143903.
[75] Watanabe H, Manabe C, Shigematsu T, Shimizu M. Applied Physics Letters 2001;78(19):2928–30.
[76] Wen ZC, Wei HX, Han XF. Applied Physics Letters 2007;91(12):122511.
[77] Jung YS, Chang JB, Verploegen E, Berggren KK, Ross CA. Nano Letters 2010; 10(3):1000–5.
[78] Jung YS, Lee JH, Lee JY, Ross CA. Nano Letters 2010;10(9):3722–6.
[79] Bita I, Yang JKW, Jung YS, Ross CA, Thomas EL, Berggren KK. Science 2008; 321(5891):939–43.
[80] Ro HW, Soles CL. Materials Today 2011;14(1–2):20–33.
[81] Yang JKW, Jung YS, Chang JB, Mickiewicz RA, Alexander-Katz A, Ross CA, et al. Nature Nanotechnology 2010;5(4):256–60.
[82] Tavakkoli KGA, Gotrik KW, Hannon AF, Alexander-Katz A, Ross CA, Berggren KK. Science 2012;336(6086):1294–8.
[83] Dawes K, Glover L, Vroom D. The effects of electron beam and g-irradiation on polymeric materials physical properties of polymers handbook. New York: Springer; 2007. p. 867–87.
[84] Son JG, Chang JB, Berggren KK, Ross CA. Nano Letters 2011;11(11):5079–84.
[85] Jeong JW, Park WI, Kim M-J, Ross CA, Jung YS. Nano Letters 2011;11(10): 4095–101.
[86] Baney RH, Itoh M, Sakakibara A, Suzuki T. Chemical Reviews 1995;95(5): 1409–30.
[87] Cordes DB, Lickiss PD, Rataboul F. Chemical Reviews 2010;110(4):2081–173.
[88] Laine RM. Journal of Materials Chemistry 2005;15(35–36):3725–44.
[89] Tegou E, Bellas V, Gogolides E, Argitis P, Eon D, Cartry G, et al. Chemistry of Materials 2004;16(13):2567–77.
[90] Hayakawa T, Seino M, Goseki R, Hirai T, Kikuchi R, Kakimoto M, et al. Polymer Journal 2006;38(6):567–76.
[91] Hirai T, Leolukman M, Hayakawa T, Kakimoto M, Gopalan P. Macromolecules 2008;41(13):4558–60.
[92] Hirai T, Leolukman M, Liu CC, Han E, Kim YJ, Ishida Y, et al. Advanced Materials 2009;21(43):4334–8.
[93] Tada Y, Yoshida H, Ishida Y, Hirai T, Bosworth JK, Dobisz E, et al. Macromolecules 2012;45(1):292–304.
[94] Reichmanis E, Smolinsky G. Proceedings of the Society of Photo-Optical Instrumentation Engineers 1984;469:38–44.
[95] Fukukawa K, Zhu L, Gopalan P, Ueda M, Yang S. Macromolecules 2005;38(2): 263–70.
[96] Ku SJ, Kim SM, Bak CH, Kim J-B. Polymer 2011;52(1):86–90.
[97] Cushen JD, Otsuka I, Bates CM, Halila S, Fort S, Rochas C, et al. ACS Nano 2012;6(4):3424–33.
[98] Jakubowski W, Kirci-Denizli B, Gil RR, Matyjaszewski K. Macromolecular Chemistry and Physics 2008;209(1):32–9.
[99] Freer EM, Krupp LE, Hinsberg WD, Rice PM, Hedrick JL, Cha JN, et al. Nano Letters 2005;5(10):2014–8.
[100] Sundström L, Krupp L, Delenia E, Rettner C, Sanchez M, Hart MW, et al. Applied Physics Letters 2006;88(24):3.
[101] Kim H-C, Rettner CT, Sundström L. Nanotechnology 2008;19(23):235301.
[102] Park SM, Park OH, Cheng JY, Rettner CT, Kim H-C. Nanotechnology 2008; 19(45):6.
[103] Cheng JY, Pitera J, Park OH, Flickner M, Ruiz R, Black CT, et al. Applied Physics Letters 2007;91(14):3.
[104] Chuang VP, Jung W, Ross CA, Cheng JY, Park OH, Kim H-C. Journal of Applied Physics 2008;103(7):5.
[105] Park OH, Cheng JY, Hart MW, Topuria T, Rice PM, Krupp LE, et al. Advanced Materials 2008;20(4):738–42.
[106] Kim DH, Sun ZC, Russell TP, Knoll W, Gutmann JS. Advanced Functional Materials 2005;15(7):1160–4.
[107] Kim DH, Kim SH, Lavery K, Russell TP. Nano Letters 2004;4(10):1841–4.
[108] Kim HC, Jia X, Stafford CM, Kim DH, McCarthy TJ, Tuominen M, et al. Advanced Materials 2001;13(11):795–7.
[109] Melde BJ, Burkett SL, Xu T, Goldbach JT, Russell TP, Hawker CJ. Chemistry of Materials 2005;17(18):4743–9.
[110] Tseng Y-C, Peng Q, Ocola LE, Elam JW, Darling SB. The Journal of Physical Chemistry C 2011;115(36):17725–9.
[111] Chen JY, Wiley BJ, Xia YN. Langmuir 2007;23(8):4120–9.
[112] Kline TR, Tian ML, Wang JG, Sen A, Chan MWH, Mallouk TE. Inorganic Chemistry 2006;45(19):7555–65.
[113] Knight MW, Grady NK, Bardhan R, Hao F, Nordlander P, Halas NJ. Nano Letters 2007;7(8):2346–50.
[114] Ieong M, Doris B, Kedzierski J, Rim K, Yang M. Science 2004;306(5704): 2057–60.
[115] Wei ZQ, Zamborini FP. Langmuir 2004;20(26):11301–4.
[116] Wu Y, Xiang J, Yang C, Lu W, Lieber CM. Nature 2004;430(7000):704.
[117] Xia YN, Yang PD, Sun YG, Wu YY, Mayers B, Gates B, et al. Advanced Materials 2003;15(5):353–89.
[118] Xu QB, Bao JM, Capasso F, Whitesides GM. Angewandte Chemie – International Edition 2006;45(22):3631–5.
[119] Chiu JJ, Kim BJ, Kramer EJ, Pine DJ. Journal of the American Chemical Society 2005;127(14):5036–7.
[120] Park SC, Kim BJ, Hawker CJ, Kramer EJ, Bang J, Ha JS. Macromolecules 2007; 40(22):8119–24.
[121] Kim BJ, Bang J, Hawker CJ, Kramer EJ. Macromolecules 2006;39(12): 4108–14.
[122] Grubbs RB. Polymer Reviews 2007;47(2):197–215.
[123] Krishnamoorthy S, Hinderling C, Heinzelmann H. Materials Today 2006;9(9): 40–7.
[124] Li MQ, Ober CK. Materials Today 2006;9(9):30–9.
[125] Spatz JP, Herzog T, Mossmer S, Ziemann P, Moller M. Advanced Materials 1999;11(2):149–53.
[126] Chai J, Wang D, Fan XN, Buriak JM. Nature Nanotechnology 2007;2(8): 500–6.
[127] Chai J, Buriak JM. ACS Nano 2008;2(3):489–501.
[128] Fernandez-Nieves A, Fernandez-Barbero A, Vincent B, de las Nieves FJ. Macromolecules 2000;33(6):2114–8.
[129] Loxley A, Vincent B. Colloid and Polymer Science 1997;275(12):1108–14.
[130] Zhang X, Harris KD, Wu NLY, Murphy JN, Buriak JM. ACS Nano 2010;4(11): 7021–9.
[131] Wu NLY, Zhang X, Murphy JN, Chai JA, Harris KD, Buriak JM. Nano Letters 2012;12(1):264–8.
[132] Kulbaba K, Manners I. Macromolecular Rapid Communications 2001;22(10): 711–24.
[133] Whittell GR, Hager MD, Schubert US, Manners I. Nature Materials 2011; 10(3):176–88.
[134] Lammertink RGH, Hempenius MA, Chan VZH, Thomas EL, Vancso GJ. Chemistry of Materials 2001;13(2):429–34.
[135] Lammertink RGH, Hempenius MA, van den Enk JE, Chan VZH, Thomas EL, Vancso GJ. Advanced Materials 2000;12(2):98–103.
[136] Eloi JC, Chabanne L, Whittell GR, Manners I. Materials Today 2008;11(4): 28–36.
[137] Whittell GR, Manners I. Advanced Materials 2007;19(21):3439–68.
[138] Korczagin I, Lammertink RGH, Hempenius MA, Golze S, Vancso GJ. Advances in Polymer Science 2006;200:91–117.
[139] Roerdink M, Hempenius MA, Vancso GJ. Chemistry of Materials 2005;17(6): 1275–8.
[140] Eitouni HB, Balsara NP, Hahn H, Pople JA, Hempenius MA. Macromolecules 2002;35(20):7765–72.
[141] Cheng JY, Zhang F, Chuang VP, Mayes AM, Ross CA. Nano Letters 2006;6(9): 2099–103.
[142] Chuang VP, Cheng JY, Savas TA, Ross CA. Nano Letters 2006;6(10): 2332–7.
[143] Roerdink M, Hempenius MA, Gunst U, Arlinghaus HF, Vancso GJ. Small 2007; 3(8):1415–23.
[144] Lu J, Chamberlin D, Rider DA, Liu M, Manners I, Russell TP. Nanotechnology 2006;17(23):5792–7.
[145] Chuang VP, Ross CA, Gwyther J, Manners I. Advanced Materials 2009;21(37): 3789–93.
[146] Podbielski J, Giesen F, Grundler D. Physical Review Letters 2006;96(16): 167207.
[147] Aharonov Y, Bohm D. Physical Review 1959;115(3):485–91.
[148] Lévy LP, Dolan G, Dunsmuir J, Bouchiat H. Physical Review Letters 1990; 64(17):2074–7.
[149] Yu LW, Chen KJ, Song J, Xu J, Li W, Li XF, et al. Physical Review Letters 2007; 98(16):166102.
[150] Chuang VP, Gwyther J, Mickiewicz RA, Manners I, Ross CA. Nano Letters 2009;9(12):4364–9.
[151] Son JG, Gwyther J, Chang J-B, Berggren KK, Manners I, Ross CA. Nano Letters 2011;11(7):2849–55.
[152] Choi HK, Gwyther J, Manners I, Ross CA. ACS Nano 2012;6(9):8342–8.
[153] Cao L, Massey JA, Winnik MA, Manners I, Riethmüller S, Banhart F, et al. Advanced Functional Materials 2003;13(4):271–6.
[154] Rider DA, Liu K, Eloi J-C, Vanderark L, Yang L, Wang J-Y, et al. ACS Nano 2008; 2(2):263–70.

Adam Nunns graduated with an MSci in Chemistry from the University of Bristol, in 2009. He is currently studying for a PhD with Prof. Ian Manners, with research orientated towards developing metallopolymer-based block copolymer materials for the use in block copolymer lithography.

Jessica Gwyther studied at the University of Bristol, graduating with an MSci in Chemistry in 2007. After her degree, she obtained a PhD in 2011 under the supervision of Prof. Ian Manners focusing on the synthesis, characterization and thin film self-assembly of metal-containing polymers. She is currently a postdoctoral fellow in the same group working on crystallization-driven self-assembly of block copolymers.

Ian Manners received his Ph.D. from the University of Bristol in 1985 in the area of transition metal chemistry. He conducted postdoctoral work in Germany in main group chemistry and in the USA on polymeric materials. He joined the University of Toronto, Canada in 1990 and after 15 years returned to his Alma Mater to take up a Chair in Inorganic, Macromolecular and Materials Chemistry, in 2006. His research interests focus on the development of new synthetic approaches and their applications in molecular synthesis, polymer and materials science, supramolecular chemistry, and nanoscience.